TOOL MOTION DIFFERENCES BETWEEN EXPERTS AND NOVICES IN LAPAROSCOPIC SURGERY

Farzad Aghazadeh[1], Bin Zheng[2], Mahdi Tavakoli[3], Hossein Rouhani[1*]
[1]Department of Mechanical Engineering, [1]University of Alberta, [2]Department of Surgery, [2]University of Alberta, [3]Department of Electrical and Computer Engineering, [3]University of Alberta
email: hrouhani@ualberta.ca

Introduction

Minimally invasive surgeries such as laparoscopic surgery are more difficult to perform compared to open surgeries due to the fulcrum effect of tools and limited tactile feedback; hence, a rigorous skill assessment is needed to ensure one's proficiency. Surgical skill assessment has significantly relied on checklists such as Objective Structured Assessment of Technical Skill (OSATS) [1] and Global Operative Assessment of Laparoscopic Skills (GOALS) [2]; however, these checklists are subjective and require experts to evaluate them based on observations. Objective methods have the potential to outperform the current subjective and labor-intensive checklists.

Motion analysis constitutes a predominant part of these checklists. Nevertheless, motion tracking in minimally invasive surgeries is more challenging than open surgeries due to the tooltip occlusion. In this study, we propose to use marker-based motion tracking, which eliminates the need for image-processing [3], which is complex and sensitive to light. Our proposed method offers 3D position data compared to 2D video recordings [4].

Methods

Five novices without any general surgery background and three expert surgeons with extensive experience in laparoscopic surgery participated in this study. Each participant underwent two tasks: (i) Peg transfer, one of the Fundamentals of Laparoscopic Surgery (FLS) tasks and (ii) dual transfer tasks, both repeated in five trials, resulting in overall ten trials per participant. The order of tasks execution was randomized.

Three markers were placed on each surgical tool (Figure 1). Motion metrics such as path length, path length along instrument axis, standard deviation of path length, mean velocity and dimensionless jerk (motion smoothness index) were derived to elucidate differences among experts and novices.

Considering a small sample size of the experts' group, we selected a nonparametric statistical test, the Mann-Whitney U test, to investigate the significant differences between motion metrics in the two groups (significance level: $p<0.05$).

Results and Discussion

(A) (B)

Figure 1: Simulated laparoscopic surgical setting: (A) box, laparoscope, surgical graspers and monitor (B) surgical grasper

Table 1 shows the mean and standard deviation for each metric. Experts had significantly shorter path length, better depth perception (lower Dpathx and NDpathx), lower path length variability among trials, and smoother movements. Experts also showed higher mean velocity for the dominant instrument in dual transfer and the non-dominant instrument in peg transfer task.

Experts accomplished the trials with significantly shorter movements, resulting in lower path length in 3D and lower path length along the instrument axis (i.e., better economy of motion). Additionally, they performed the tasks more consistently, indicated by a smaller standard deviation of path length among repetitions (DpathSD and NDpathSD). Smaller dimensionless jerk (Dsmooth and NDsmooth) showed that experts offered smoother movements compared to novices.

Table 1: Motion metrics of expert and novice groups for peg transfer and dual transfer tasks

Metric	Dpath (m)	NDpath (m)	Dpathx (m)	NDpathx (m)	DpathSD (m)	NDpathSD (m)	Dvel (cm/s)	NDvel (cm/s)	Dsmooth/10^7 -	NDsmooth/10^7 -
Novices_peg	2.97(0.63)	3.40(0.45)	1.14(0.17)	1.35(0.24)	0.68(0.28)	1.02(0.39)	2.90(0.41)	3.30(0.24)	3.94(1.65)	4.30(1.55)
Experts_peg	1.49(0.21)	1.61(0.21)	0.75(0.17)	0.72(0.20)	0.20(0.07)	0.18(0.16)	3.60(0.54)	3.85(0.51)	0.47(0.03)	0.49(0.03)
Novices_dual	1.98(0.47)	2.49(0.71)	0.73(0.14)	0.95(0.28)	0.45(0.16)	0.84(0.81)	2.76(0.52)	3.38(0.43)	2.24(1.66)	2.38(1.79)
Experts_dual	0.96(0.26)	0.94(0.23)	0.48(0.11)	0.42(0.13)	0.13(0.08)	0.13(0.05)	3.86(0.79)	3.70(0.65)	0.15(0.03)	0.17(0.03)

Values are expressed as mean (standard deviation), D: dominant, ND: non-dominant, SD: standard deviation, path: path length, pathx: path length along instrument axis, vel: velocity, smooth: motion smoothness, for instance: NDpathSD=non-dominant path length standard deviation among five repetitions

Significance

We found promising motion metrics indexes characterizing surgical skills. These motion metrics can be used to classify skill levels which can benefit healthcare society with the advantages of objectivity and a drastic reduction in experts' invested time for skill assessment and training.

References

[1] Martin et al., *1997, British J Surgery, 10.1046*
[2] Vassiliou et al., 2005, *American J Surgery*, 10.1016
[3] Baghdadi et al., 2019, *ICARS*, 10.1007
[4] Azari et al., 2020, *Applied Ergonomics*, 10.1016

QUANTIFYING ARM FUNCTION AFTER BREAST RECONSTRUCTION WITH REAL-WORLD REACHING TASKS

Kathylee Pinnock Branford[1*], Jordan Kartes[2], Jordyn Ingber[2], Lauren Sickmiller[2], Athena Prine[2], David B. Lipps[2], Stephen M. Cain[1]
[1]West Virginia University, Morgantown, WV and [2]University of Michigan, Ann Arbor, MI
email: kp0107@mix.wvu.edu

Introduction

In the U.S, more breast cancer patients are opting for a mastectomy followed by breast reconstruction [1]. Breast reconstruction patients commonly report limitations in shoulder mobility in the months following surgery [2]. Knowledge about how shoulder morbidities associated with mastectomy and reconstruction impact everyday use of the arm is limited to subjective patient-reported outcome surveys. Quantitative measures of arm movement quality are important for distinguishing healthy and reduced functionality. Existing approaches used to objectively evaluate arm movement are employed in laboratory settings and require specialized instrumentation to track movements [3,4]. Enabling quantitative approaches that can be utilized in out-of-the-lab settings is necessary to evaluate real-world arm function. This preliminary study aimed to develop an inertial measurement unit (IMU) based approach for evaluating activities of daily living and to explore which tasks are most useful for evaluating arm movement and whether IMU-derived measures of function are sensitive to manual asymmetries or cancer status.

Methods

Ten female subjects (mean±SD age 54.4±5.3 years) provided written consent to participate in this University of Michigan IRB-approved study. Four breast cancer patients (each had bilateral mastectomy and reconstruction) and six healthy matched control patients were evaluated. Data were collected at the University of Michigan HomeLab, a fully functional apartment where participants were observed performing activities of daily living (ADLs). Each participant wore five IMUs (APDM Opal; sampling rate: 128 Hz): one on each wrist, one above each elbow, and one above the sternum. We focused on three tasks: reaching for a can on a high shelf (*high reach*), lifting a can to a low shelf (*low lift*), and lifting a can to a high self (*high lift*). Participants performed each task twice with both their dominant arm and nondominant arm. We calculated the velocity and position of each wrist from the raw IMU data using a ZUPT algorithm [5]. Forearm, upper arm, and thorax elevation angles were estimated from the IMU data [6]. Wrist heights relative to the shoulder joint were calculated from segment elevation angles [7]. This study focused on six metrics that have been used to evaluate reaching tasks (Figure 1): linearity of the forearm elevation angle - upper arm elevation angle - wrist height trajectory (*Linearity*), linearity of the wrist position trajectory (*Position Linearity*), duration of the reach (*Duration*), peak wrist velocity (*Peak Velocity*), time to peak velocity (*Time to Peak*), and time after peak velocity (*Time after Peak*). We used generalized linear models to explore the effects of arm (dominant or non-dominant), cancer status, and the interaction of arm and cancer status on the calculated metric

Results and Discussion

Results are summarized in Figure 1. Cancer status alone had no significant effect on the metrics for any task. In the *high lift*, use of the dominant arm was associated with decreased *Linearity* (p=0.009), *Position Linearity* (p=0.001), and *Peak Velocity* (p=0.006), but longer *Duration* (p=0.024) and *Time to Peak* (p=0.017). Use of the dominant arm in cancer patients in the *high lift* was associated with longer duration reaches (p=0.014). In the *high reach*, the use of the dominant arm in cancer patients was associated with decreased *Linearity* (p=0.038) and *Peak Velocity* (p=0.045). In the *low lift*, decreased *Peak Velocity* (p= 0.004) was associated with the use of the dominant arm of cancer patients.

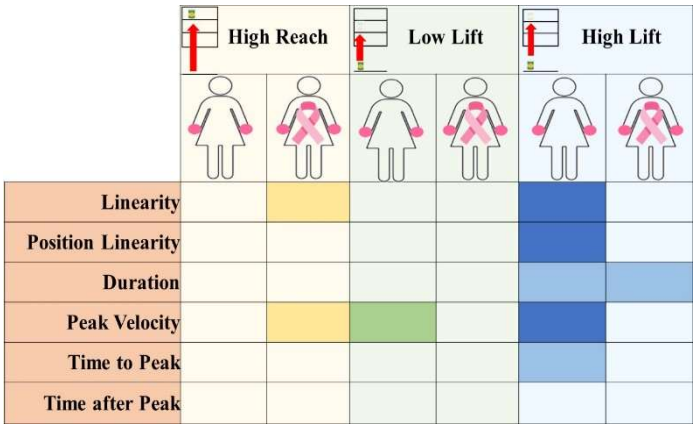

Figure 1: Effects of arm dominant vs. non-dominant (silhouette with shaded hands) and the interaction of arm and cancer status (silhouette with shaded hands and pink ribbon) on reaching metrics for three reaching tasks. Dark shades indicate p<0.01, medium shades p<0.05, and lighter colors indicate no significant effect.

Objective evaluation of real-world arm function after breast reconstruction remains an important challenge. Real-world reaching tasks do not have precisely defined starting and ending locations or known goals. Reaching metrics used for laboratory studies can be calculated from IMU data and used to evaluate real-world reaching tasks. These metrics revealed manual asymmetries similar to laboratory studies [4],. Arm dominance had the most effect on the *high lift* task, suggesting that some reaching tasks are more sensitive to changes in arm function. Future work will explore additional reaching metrics.

Significance

Real-world reaching tasks can be captured by worn IMUs and objectively evaluated with IMU-based calculations of reaching metrics similar to those employed in laboratory studies. Reaching metrics from a challenging reaching task (lifting a can to a high shelf) are most sensitive to manual asymmetries, suggesting they will be useful for tracking changes in arm function over time.

Acknowledgments

This project was funded by NIH/NICHD R03HD097704 and the U-M School of Kinesiology Marie Hartwig Research Fund.

References

[1] Kummerow, K.L., et al. *JAMA Surg* (2015). [2] Tarantino, I. et al. *Plast Reconstr Surg* (2006). [3] Przybyla, A., et al. *Neurosci Lett.* (2011). [4] Sainburg and Kalakanis, J Neurophysiol (2000). [5] Rebula, J.R., et al. *Gait & Posture* (2013). [6] Savage, P.G. *J Guidance, Ctrl, Dyn* (1998). [7] Laidig, D. & Seel, T. *Current Dir Biomed. Eng.* (2017).

STEP-TO-STEP GAIT SYMMETRY IN MILD-TO-MODERATE GLAUCOMA

Natalie Bick[1*], Mark Redfern[1], Ian Conner, Gadi Wollstein, Kevin Chan, Caitlin O'Connell, Rakié Cham[1]
[1]Department of Bioengineering, University of Pittsburgh, Pittsburgh, PA
email: *nab173@pitt.edu

Introduction

Many aging-related factors contribute to falls, including balance/gait deficits and vision impairments [1]. Glaucoma is a leading cause of blindness primarily impacting older adults. Adults with glaucoma fall at a greater rate than similarly aged adults without glaucoma [2, 3]. While glaucoma-related changes in vision certainly contribute to falls, other risk factors may be at play. Gait impairments have been identified in people with glaucoma; however, they do not fully explain why greater visual field loss results in higher fall rates [4]. One reason could be that the appropriate gait characteristic related to falls in glaucoma has not yet been identified. One example is step-to-step symmetry, often quantified using the harmonic ratios (HR), which is derived based on the frequency analysis of trunk acceleration signals. HRs have been associated with falls risk in older adults [5], but have not been investigated in glaucoma. This study tested the hypothesis that step-to-step gait symmetry in the anterior-posterior (AP) and medial-lateral (ML) directions will be reduced with more severe structural (retinal nerve fiber layer; RNFL) and functional (mean-deviation of the visual fields; MD; [6]) vision changes in glaucoma. We examined step-to-step symmetry in four floor/light conditions, with and without a cognitive load.

Methods

Eleven adults (N=11, 4 male and 7 female) diagnosed with mild to moderate glaucoma were recruited, ranging in age from 54 to 80 years (mean/sd=65.5/8.2). Participants had no musculoskeletal or neurological conditions that impacted gait. A full factorial experimental design was implemented consisting of 8 walking conditions: 4 flooring/lighting conditions, with and without a cognitive load (auditory choice reaction time *task*). The flooring conditions were hard, vinyl tile floor and soft carpeted floor. The lighting conditions were well-lit (623 lux) and dimmed (3 lux). Participants were instrumented with an accelerometer (Delsys Inc, Boston, MA) attached posteriorly at the L3-L4 level, from which HRs were derived during walking at a self-selected speed [5]. Gait trials were each 3 minutes. Four mixed linear regression models were used, with one model per *eye* metric (MD Better Eye, MD Worse Eye, RNFL Better Eye, RNFL Worse Eye). Fixed effects included *eye*, *task*, *flooring/lighting* and the first order interaction effects. The dependent variables were the HRs in the AP and ML direction, separately fit. *Participant* was included as a random effect. Statistical significance was set at α=0.01 to reduce the chances of type I errors. Post-hoc student's t-tests were conducted with significance set at α=0.05.

Results and Discussion

The association of MD Better Eye and HR in the AP direction ($F(1,9)=9.6$, $p=0.01$, Figure 1) was statistically significant, with the HR decreasing (reduced symmetry) with decreasing MD Better Eye values. Similarly, lower RNFL Better Eye values were associated with decreased HR AP, and approached significance ($F(1,0)=6.8$, $p=0.03$). MD Worse Eye and RNFL Worse Eye were not significantly associated with HR AP.

The impact of *flooring/lighting* on HR AP was statistically significant ($F(3,65)=3.8$, $p=0.01$) in the model using MD Better

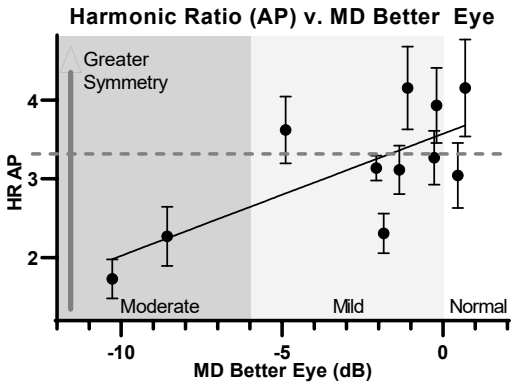

Figure 1: *HRs in the AP direction, averaged across trials. Dotted line represents the average HR AP in healthy older adults with a similar average gait speed to that of the present study (>1.15m/s) [7].*

Eye metric. Post-hoc student's t-tests revealed that Soft-Well-lit was significantly larger than Hard-Dim ($p=0.04$) and Hard-Well-lit ($p=0.007$). Additionally, Soft-Dim was significantly larger than Hard-Well-lit ($p=0.01$). The overall trend was increased HR APs on carpeted floor, with no overall trend with lighting. The interaction of MD Better *Eye* and *flooring/lighting* was not significant.

The interaction of *flooring/lighting* and *eye* was significantly associated with HR ML in the MD Worse Eye ($F(3,65)=5.4$, $p=0.002$) and RNFL Worse Eye ($F(3,65)=4.5$, $p=0.006$) models. Cognitive *task* had no significant impact on any dependent variable.

These results indicate that gait symmetry in the AP direction was reduced with greater visual field loss, and potentially greater structural loss, in mild-moderate glaucoma. Floor conditions also impacted harmonic ratios in this sample, regardless of vision loss.

Significance

The findings of this study show that gait symmetry may be an important metric in understanding the mechanisms of gait deficits in people with glaucoma, and further work is needed to determine if gait symmetry is associated with increased falls risk in people with glaucoma. Further work with individuals with moderate and severe glaucoma is also needed.

Acknowledgments

NIH / NEI, "Effects of Visual Fields on Standing Balance" (NIH R03-AG043748); BrightFocus Foundation National Glaucoma Research Program (G2016030); NIH / NEI, "Novel Glaucoma Diagnostics for Structure and Function" (NIH R01-EY013178); Unrestricted grant from Research to Prevent Blindness

References

[1]Ambrose et al., 2013. *Maturitas*. 75(1): 51-61 [2]Lamoureux et al., 2008. *Invest Ophthalmol Vis Sci*. 49(2): 528-33. [3]Ramulu, 2009. *Curr Opin Ophthalmol*. 20(2): 92-8. [4]Mihailovic et al., 2020. *Invest Ophthalmol Vis Sci*, 61(3): 30. [5]Bellanca et al., 2013. *J Biomech.* 46(4): 828-31. [6]Kanamori et al., 2003. *Am J Of Ophthalmol.* 135(5): 513-520. [7]Brach et al., 2011. *J of Geront.* 66A(1): 136-141

HUMAN EARCANAL DYNAMIC MOTION: A DISCRETE APPROACH TO STUDY THE SIZE AND SHAPE VARIATIONS WITH HEAD, FACE AND JAW MOVEMENTS

Michel Demuynck[1*], Aidin Delnavaz[1], Jérémie Voix[1]
[1]Department of Mechanical Engineering, École de technologie supérieure, Université du Québec, Montréal, QC H3C 1K3, Canada
email: *michel.demuynck.1@ens.etsmtl.ca

Introduction

The human earcanal (EC) is subject to size and shape variations due to head, face and jaw movements. Several studies proved that a significant amount of energy can be harvested from such activities. The complexity of the EC anatomy makes in vivo measurements impossible to identify accurately the locations where an in-ear energy harvester should be placed. Although in situ [1,2] or analytical studies [3] have already evaluated the power capability of earcanal dynamic motion, it is still hard to estimate how much these studies are accurate in terms of predicting the locations where the energy capability of the earcanal is maximum. The purpose of this study is to compute the earcanal dynamic motion for different head, face and jaw movements among healthy subjects in order to identify the EC regions that would provide the highest amount of harvestable energy.

Methods

Thirty four healthy subjects (10 females, 24 males), aged 17 to 59 (32.5 [26 ; 39] years old) participated in this study. Five activities were considered on both ears for each subject and their ear impressions were taken. All the earmolds were scanned and discretized in 11 cross-sections (CS) as illustrated in Fig. 1. For each subject, the closed-mouth (CM) EC model was considered as the reference.

Six CS-related geometrical parameters were computed: area (A), perimeter (P), longest (D_{max}) and shortest (D_{min}) diameters, circularity (c), aspect ratio (r). A statistical analysis was performed to evaluate size and shape differences between the CM-EC and 4 other activities.

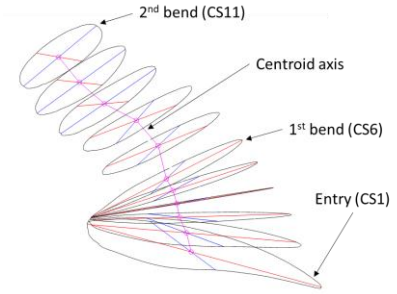

Figure 1: Earcanal discretization (black line) in 11 CS (numbered CS1 to CS11) with D_{max} (red line) and D_{min},(blue line), and the centroid axis (purple line) from the entry to the second bend planes

Results

Figure 2 shows that during mouth opening (MO), raising eyebrows (RE) and smiling (SM), EC contracts at the entry but then only MO-EC tends to expand from first bend. Only MO-EC contracts significantly ($\%\Delta A_{min}$ = -4.67% [-6,57; -2.30] at CS1, p<0.001), while both MO ($\%\Delta A_{max}$ = 3.57% [1.68;5.47] at CS8, p<0.001) and SM-EC ($\%\Delta A_{max}$ = 7.51% [1.43;14.35] at CS8, p<0.001) expand significantly. Turning head left (THL) tends to expand EC from entry to 2nd bend ($\%\Delta A_{max}$ = 4.12% [-2.70;8.65] at CS8, p>0.05) but only significantly before 1st bend.

The CS shape does not change much until first bend for MO, THL and RE-EC, while SM-EC is significantly more elliptical ($\%\Delta r_{max}$ = 9.25% [2.76;15.32] at CS4, p<0.001). All the EC tend to be more circular until the second bend, but only significantly for MO ($\%\Delta r_{min}$ = -4.44% [-7.61;2.65] at CS8, p<0.001) and SM-EC ($\%\Delta r_{min}$ = -6.47% [-10.67;-0.14] at CS9, p<0.001).

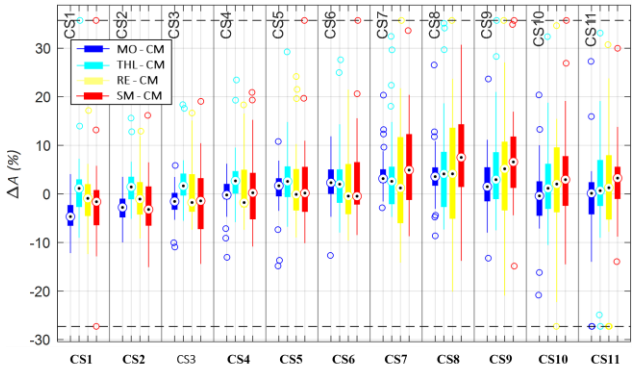

Figure 2: Area differences (%) regarding to CM position

Discussion

MO and SM show the highest differences in size and shape. The transition between first and second bend (CS7-CS8) looks like a turning point as area and aspect ratio differences change sign at this location. The proximity of the mandibular condyle could explain this fact. Several studies show that the mechanical coupling between TMJ and EC is located between the two bends [4,5,6]. By placing an energy harvester between first and second bends, MO and SM should provide a significant amount of energy resulting from contraction and expansion of the EC.

Acknowledgments

The authors would like to acknowledge the support of Natural Sciences and Engineering Council of Canada (NSERC) through the last author's Discovery grant (RGPIN-2017-06192). The technical support received from EERS Global Technologies through the NSERC-EERS Industrial Research Chair in In-Ear Technologies (CRITIAS) is also greatly appreciated.

References

[1] Bouchard-Royet al., 2020. *IEEE Sensors Journal,* 20 (12): 6338–45. 10.1109/JSEN.2020.2976925.
[2] Delnavaz et al., 2013. *Journal of Applied Physics,* 113 (6): 064701. 10.1063/1.4792307.
[3] Carioli et al., 2016. *AIP Advances,* 6 (12): 125203. 10.1063/1.4971215.
[4] Darkner et al., 2007. *Internal Conference on Medical Image Computing and Computer-Assisted Intervention,* 4792: 801–8. 10.1007/978-3-540-75759-7_97.
[5] Pirzanski. 2006. *Hearing Review*, 13(5), 39.
[6] Oliveira et al., 2005. *Hearing Review* 12 (2): 18-19.

IN-VIVO MEASUREMENT OF SPINOUS PROCESS SEPARATION DURING AXIAL DISTRACTION

Maruti R. Gudavalli[1*], Ralph D. Kruse[1], Bret A. White[1], and Stacey L. Rider[2]
[1]Keiser University College of Chiropractic Medicine, West Palm Beach Campus
[2] Program Director, Diagnostic Medical Sonography Program, Southeastern College, West Palm Beach
email: *mgudavalli@keiseruniversity.edu

Introduction

Low back pain (LBP) is a burden to society in terms of disability, lost workdays, and costs. Although Spinal Manipulative Therapy (SMT) is beneficial in helping LBP patients, the mechanism of SMT is not well understood. One hypothesis is SMT restores intersegmental movements. Ultrasound measurement of spinous process separation can be useful to assess the intersegmental movements. Our long-term objective is to understand the mechanism of interspinous process separation during chiropractic procedures and its effects on low back pain. The objective of this study was to quantify the separation of spinous process separation during axial distraction of lumbar spine under 12lb (53.4N) and 25lb (111.2N) traction force using Cox flexion-distraction treatment protocol.

Methods

This study was approved by the Institutional Review Board (IRB). To achieve our objective, we recruited 30 volunteers who did not have low back pain and were generally healthy. **Mean age**: *32.4 years* **Mean weight**: *69.21 kg* **Mean Height**: *169.6 cm* **Sex**: *Male: 16; Female: 14*
The volunteers were asked to lie prone on a chiropractic flexion-distraction table. An ultrasound imaging sonographer performed scanning *(GE Model LOGIQ P9)* to image the spinous processes from L3-S1 under no load. The volunteers were distracted using the Cox flexion distraction table in automated setting of 12 lbs (53.4N) of traction and 25 lbs (111.2N) of traction. Ultrasound images (Figure 1) were collected at these two loading conditions. The increase in the separation of spinous process were measured at 12lbs and 25lbs compared to no loading conditions. Measurements were made and recorded by identifying the tips of the spinous processes and distances between L3-L4, L4-L5, and L5-S1. Descriptive statistics on the separation in terms of mean and standard deviation were calculated.

Table 1. Spinous process separation (mm) at L5-S1, L4-L5, and L3-L4

N=30	L5-S1	L4-L5	L3-L4
Initial separation	15.9 (2.5)	24.5(3.2)	26.6(2.5)
Increase in separation under 12lbs (53.4N)	1.27(0.9)	1.25(0.8)	1.28(1.16)
Increase in separation under 25lbs (111.2N)	1.98(1.0)	2.24(0.99	1.94(1.36)

Figure 1: A photograph of volunteer in prone position, experienced sonographer performing an ultrasound scan of the lumbar spine.

Results and Discussion

Table 1 provides the data on the initial separation, increase in separation under 12lbs and 25lbs of traction application for all three levels of lumbar spine (L5-S1, L4-L5, and L3-L4). Initial separation is higher at L3-L4, followed by L4-L5, and L5-S1. Increase in separation is similar at all three levels with mean increase of 1.25-1.28mm under traction load of 12lbs. Increase in the separation distance is slightly higher at L4-L5 under 25lbs of traction load. This study reports on the in vivo measurement of spinous process separation while administering automated axial traction using the Cox flexion-distraction table. Cox flexion-distraction technique is used to treat low back pain patients and has demonstrated clinical improvement in randomized clinical trials. The results from this study will provide some mechanistic approach in studying the movements of vertebra by measuring spinous process separation. The present study is limited to healthy volunteers without low back pain. Future studies involving low back pain patients are planned.

Significance

This study demonstrates the importance of measuring movements inter-segmentally in the lumbar spine that will provide insights into the mechanisms of chiropractic traction procedures administered by Doctors of Chiropractic. Ultrasound measurements can be a valuable tool in understanding the mechanisms of manual therapy.

Acknowledgments

Acknowledge donations from several Doctors of Chiropractic for donating for this research. Assistance from Mr. Jason Klamson in assisting with the data organization for this project.

CALCIUM SENSITIVITY OF RAT VASTUS INTERMEDIUS MUSCLE FIBRES FOLLOWING FOUR WEEKS OF DOWNHILL RUNNING

Emma F. Hubbard[1*], Avery Hinks[1], Parastoo Mashouri[1] and Geoffrey A. Power[1]
[1]Department of Human Health and Nutritional Sciences, University of Guelph, Guelph, Ontario, Canada
email: *ehubbard@uoguelph.ca

Introduction

Eccentric training has been shown to improve muscle function independent of contraction mode [1,2]. Architectural and strength adaptations have also been observed in skeletal muscle following eccentric training, with mechanistic differences from those produced by concentric training [2]. It has been suggested that increased maximal isometric force production in rodents following eccentric training may be related to improved Ca^{2+} handling [3]. However, little is known regarding the effects of eccentric training on Ca^{2+} sensitivity in single muscle fibres.

The present study aimed to identify whether Ca^{2+} sensitivity is altered in vastus intermedius (VI) single muscle fibres from eccentrically trained compared to untrained rats, and to identify any alterations in single fibre mechanical function following eccentric training. It was hypothesized that weighted downhill running training would result in greater absolute force production and that Ca^{2+} sensitivity would be higher in fibres from trained rats compared to control rats.

Methods

11 adult male Sprague-Dawley rats were split into two groups: eccentric training (n=5) or sedentary control (n=6). The eccentric training group underwent 4 weeks of training consisting of 35 minutes of downhill running 3 days/week in 5-minute bouts. Weight was applied to enhance eccentric loading, progressing from 5 to 15% body mass, using a custom-made vest.

Following sacrifice, VI muscles were harvested and chemically permeabilized. Single fibres were isolated and tied between a length controller and a force transducer, then transferred to a pre-activating solution for 20 seconds, followed by one of 7 activating solutions (pCa 7.0, 6.6, 6.4, 6.2, 5.7, 5.5, 4.5) for 30 seconds [4]. Active force (P_o) was measured at each pCa level and the pCa level at which 50% of P_o was elicited (pCa_{50}) was used to determine differences in Ca^{2+} sensitivity. Rate of force redevelopment (k_{tr}) was assessed at maximal pCa by a rapid shortening of the fibre, followed by a rapid re-stretch. Active instantaneous stiffness was measured to assess the proportion of attached cross-bridges. Following mechanical testing, fibre type was determined via SDS-PAGE.

Results and Discussion

Single fibre cross sectional area (CSA) was greater in VI muscle fibres from trained rats (~28%, P>0.05) compared to control rats. However, there was no difference in absolute or specific force between groups or fibre types. This indicates that despite the difference in fibre size between groups, there was no concomitant increase in force production in the trained muscle fibres.

As expected, there was an effect of fibre type with type II fibres producing faster k_{tr} (~330%, P<0.001) compared to type I fibres. There was no difference in active stiffness between groups or fibre types.

There was no significant difference in pCa_{50} between control and trained fibres, which would indicate that Ca^{2+} sensitivity was not altered by eccentric training. However, when considering normalized force across pCa values, there was an interaction of training group × fibre type such that type I fibres from the control group produced greater force (~20%, P<0.05) than type I fibres from the training group at lower Ca^{2+} concentrations (pCa 7.0-6.2) (Figure 1). Additionally, there was an effect of group with control fibres producing greater forces (~17%, P<0.05) at lower Ca^{2+} concentrations. There were no differences across groups or fibre types at higher Ca^{2+} concentrations (pCa 5.7-4.5).

There does not appear to be an effect of eccentric training on any of the reported mechanical measures, nor on Ca^{2+} sensitivity in rat VI muscle fibres. In fact, Ca^{2+} sensitivity may have been impaired by training, particularly at lower concentrations of Ca^{2+}. These findings suggest that changes to Ca^{2+} sensitivity are not a likely contributor to reports of improved muscle function following eccentric training.

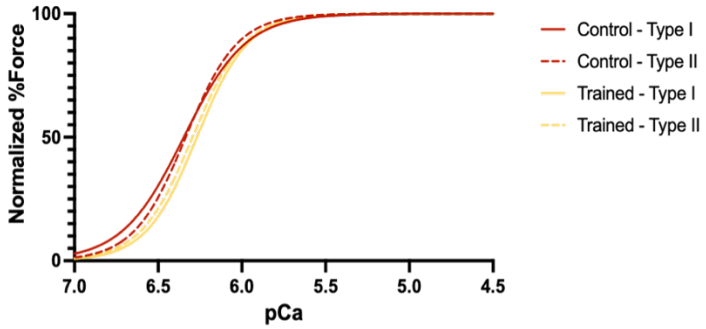

Figure 1: Normalized force across pCa levels for vastus intermedius single muscle fibres from sedentary control (red), and eccentrically trained (yellow) rats, separated by fibre type: MHC I (solid line) and MHC II (dotted line).

Significance

Eccentric training is a strong stimulator of functional adaptation while being less metabolically demanding, providing a suitable interventional tool for individuals with lower exercise capacities. However, the mechanisms of improved skeletal muscle function following eccentric training are poorly understood. Our research shows that alterations in Ca^{2+} sensitivity are likely not involved in eccentric training-induced adaptations, thereby ruling out a potential mechanism and bringing us one step closer to understanding the pathway through which eccentric training improves muscle function.

Acknowledgments

Supported by NSERC.

References

[1] Douglas et al., 2017. *Sports Med.* 47(5): 917-941.
[2] Franchi et al., 2014. *Acta Physiol Scand.* 210(3): 642-654.
[3] Willems & Stauber, 2002. *Med Sci Sports Exerc.* 34(11): 1738-1743.
[4] Mashouri et al., 2021. *Physiol Rep.* 9(2): 14725.

Gastrocnemius force-length properties in ice hockey players

Cameron D. Leonard and John H. Challis*
Biomechanics Laboratory, The Pennsylvania State University, University Park, PA 16802, USA
email: *jhc10@psu.edu

Introduction

The force-length properties of isolated muscle are well established [1], but *in vivo* only a portion of the force-length curve may be expressed. *In vivo* the manifestation of the force-length curve is seen in the joint moment, which depends on the forces produced by all of the muscles which cross a joint and the moment arms of those muscles about that joint. There is evidence that depending on the frequent joint ranges of motion the expressed section of the force-length curve can vary between subjects [2].

Ice-hockey players have constrained ankle motion due to their ice hockey skates, suggesting a potential for change in the expressed section of the gastrocnemius force-length curve compared with non-specifically trained subjects. It is feasible for bi-articular muscles, such as the gastrocnemius, to determine their force-length properties *in vivo*. Previous research has indicated non-specifically trained subjects predominantly work on the ascending limb of the force-length curve for the gastrocnemius for maximal isometric moments [3]. It is hypothesized that trained ice hockey players will have less sarcomeres in series in their gastrocnemii, which will shift these muscles to operating on the plateau region of the force-length curve. The purpose of this study was to collect data from a group of subjects to examine this hypothesis.

Methods

Twelve female Division I ice hockey players were recruited for the study. All participants provided written informed consent, for procedures approved by the Institutional Review Board. Maximum isometric plantarflexion moments were measured using a Biodex System. The subjects produced these moments for ranges of both ankle and knee joint angles.

For each pair of ankle and knee joint angles the moment arm and muscle-tendon length of the gastrocnemius was computed [4]. There were three moments for a given ankle angle as measurements were made for three knee angles (90°, 120°, and 180°). For these three moments the soleus contribution was assumed to be constant since the ankle angle did not change so its length was invariant; the contribution of the gastrocnemius to the ankle joint moment varied as its length changed with knee joint angle. Therefore, the change in gastrocnemius moment can be computed due to its length change, and using the moment arm of the muscle at the ankle joint it can be expressed as a change in force. This process was repeated for six ankle joint angles (65° to 135°), allowing reconstruction of the expressed section of the force-length curve of the gastrocnemius, which was then modelled using a first- or second-order polynomial.

For each subject the expressed section of the force-length curve was identified using the location of the peak force within the analyzed range of fiber lengths using a standardized procedure [3]. Therefore, for each subject the expressed section of the force-length curve was either the ascending limb, the plateau, or the descending limb. The frequencies of expressed sections were compared using the chi-square test with the results from an earlier study [3] performed in the same lab using the same equipment and analysis methods.

Results and Discussion

For four of the subjects they could not produce a muscle moment at their ankle joints with the knee fully extended, and the ankle plantar-flexed (135°). With this joint configuration the ankle plantar-flexors had active insufficiency, the muscles are too short to be able to produce force. This suggests the optimum length of the muscle fibers was too short for the muscle to operate on a region of the force-length curve at which it could produce force.

Polynomials were fitted to the muscle-length and change in force data for the gastrocnemius (Figure 1a). From these polynomials the *in vivo* expressed section of the force-length curve was determined for each subject (Figure 1b). There was a statistically significant difference in the frequency of the expressed section of the force-length curve for the ice hockey players compared with a group of non-specifically trained subjects ($p<0.0001$). These results indicate that the tendency of the ice hockey players was to have relatively shorter gastrocnemius muscle fibers, compared with non-specifically trained subjects, thus changing the expressed section of the force-length curve.

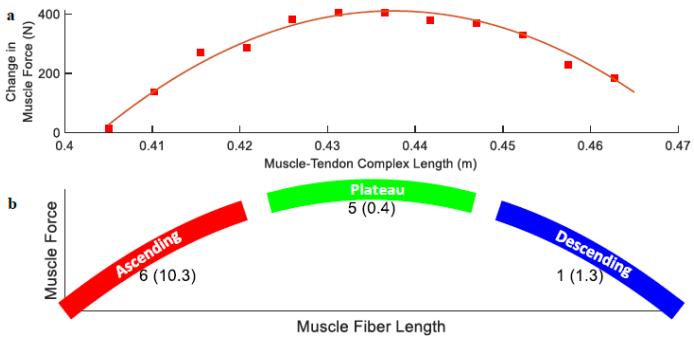

Figure 1: The force-length properties of the gastrocnemius, a) example fit to experimental data, and b) the frequency of the expressed section for each portion of the force-length curve by the subjects in this study, and in parentheses the anticipated distribution based on Winter & Challis [3].

This study indicates the expressed section of the force-length curve *in vivo* can vary between individuals and is likely influenced by the nature of the physical activity they perform.

Significance

The study presents evidence that the number of sarcomeres in series in human muscle is influenced by typical joint ranges of motion. Animal studies provide strong evidence that such a mechanism exists [e.g., 5]. These results have implications for the training of muscle whether that is for rehabilitation or sport performance improvement, as they indicate that muscle adapts to the range of motion imposed on them.

References

[1] Gordon et al. 1966. *J Physiol*. 184: 170-192.
[2] Herzog et al. 1991. *Med Sci Sports Exerc*. 23: 1289-1296.
[3] Winter & Challis. 2008. *J Appl Biomech*. 24: 207-214.
[4] Grieve et al. 1978. In: *Biomechanics VI-A*. pp. 405–412.
[5] Koh & Herzog. 1998. *J Biomech*. 31: 593-599.

BIARTICULAR MUSCLENET: A MACHINE LEARNING MODEL OF BIARTICULAR MUSCLES

Ali Nasr[1*], and John McPhee[1]
[1]Motion Research Group, Systems Design Engineering, University of Waterloo, Canada
email: *a.nasr@uwaterloo.ca

Introduction

Anatomically detailed muscle models (e.g., Hill-type muscle models) are extensively used in neuromusculoskeletal (NMSK) simulations, post-rehabilitation analysis, and biomechatronic device control. However, these models have a number of challenges, including muscle redundancy, the necessity to specify the sophisticated musculoskeletal architecture (e.g., intricate muscle wrapping routes), difficult-to-fit parameters for each muscle, parameter sensitivity, and ethically impossible verification of the muscle's variables using in vivo human tests. The Muscle Torque Generator (MTG) model recently enabled researchers to create basic independent biomechanical joint models assuming muscles are monoarticular [1]. This paper proposes a combination of MTGs [1] and MuscleNET [2] to model biarticular muscles. Precisely, Biarticular MuscleNET is a machine learning mapping of electromyography (EMG) channels to multiple MTG excitation variables simultaneously.

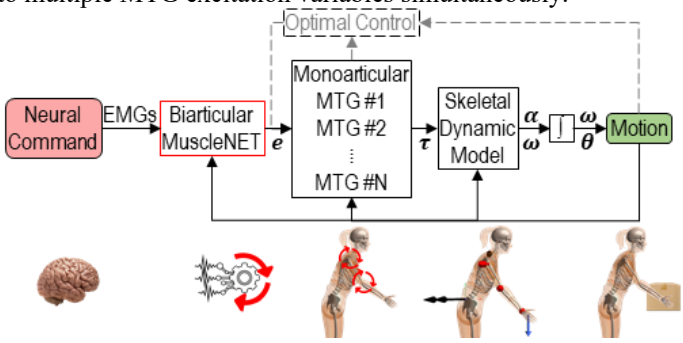

Figure 1: Schematic of typical NMSK simulation elements using Biarticular MuscleNET, monoarticular MTGs, and skeletal system. $\boldsymbol{e}$ is MTG excitations. $\boldsymbol{\tau}$, $\boldsymbol{\alpha}$, $\boldsymbol{\omega}$, and $\boldsymbol{\theta}$ are the joint moments, angular accelerations, angular velocities, and angles, respectively.

Methods

The NMSK simulation has EMG inputs and motion variable outputs and consists of three serial blocks: skeletal system, monoarticular MTGs, and Biarticular MuscleNET (Figure 1). To build and validate these models, anthropometric data, experimental data from a dynamometer, synchronized motion and EMG measuring equipment are required.

The dynamic model of the skeletal system is built with inertial and geometric parameters based on anthropometric data [3].

MTGs estimate torque-angle-velocity curves and passive components at the level of one joint. Each MTG model has a unique set of characteristics: an active component (generates the active torque limited by the joint's angle and angular velocity) and a passive component (mimicking the joint's viscosity or friction and constraining the joint range of motion). The MTG active component consists of excitation-to-activation signal function, active-torque-angular-velocity scaling function, active-torque-angle scaling function [1], and peak joint strength.

The Biarticular MuscleNET is a recurrent neural network (RNN) that uses information history (of inputs and outputs) to learn the dynamic temporal relationships of a model [2]. The RNN outputs are multiple joint excitation signals of MTGs. The RNN inputs are EMG signals, joint angles, and feedback of the outputs. One Biarticular MuscleNET estimates multiple dependent MTG excitations simultaneously and uses the estimated variables as feedback for the RNN configuration. In contrast, the monoarticular MuscleNET [2] estimates only one MTG excitation, independent of other joint variables.

To prepare the Biarticular MuscleNET's training data, first, the input signals were optimally filtered [4]. Second, the output signals or MTG excitations were calculated using the inverse dynamic simulation of the skeletal system, and finally, static optimization of redundant monoarticular MTGs.

We used data from 17 subjects (8 Males and 9 Females; 23 ± 4 years; 1.66±0.16 m height; 72 ± 30 kg mass) who were free of upper limb injuries and did pick-and-place activities in the sagittal plane. EMG signals were measured over the following right upper-limb muscles: Serratus Anterior, Supraspinatus, Infraspinatus, Pectoralis Major, Latissimus Dorsi, Anterior Deltoid, Middle Deltoid, Posterior Deltoid, Upper Trapezius, Middle Trapezius, and Lower Trapezius. The targeted joints were shoulder and elbow flexion/extension. Furthermore, the RNN consisted of one hidden layer with 40 hidden neurons, five input signal former values, and five output signal former values.

Results and Discussion

Using the prepared dataset, the regression accuracy of the RNN model (Biarticular MuscleNET) achieved 94.3, 86.3, 89.9, and 92.9% mean-square percentage of estimation for training, validation, testing, and all data sets, respectively. Comparatively, this regression accuracy is similar to the reverse estimation of the EMG signals out of kinematic and dynamic biomechanical signals when using multiple joints [5]. Coupling the joints' excitation signals (for Biarticular MuscleNET's outputs) can accomplish 3% more regression accuracy than the average monoarticular MuscleNET reported in [2].

Significance

The proposed combination of Biarticular MuscleNET and monoarticular MTGs for NMSK simulation predicted torques for an adult's pick-and-place motion comparable with experimental data. As a result, using the proposed models in NMSK simulations (Figure 1) alleviates the difficulties associated with anatomically precise muscle models.

Acknowledgments

This research was funded by the Canada Research Chairs program and the Natural Sciences and Engineering Research Council of Canada. The authors would like to acknowledge Prof. Clark R. Dickerson from the University of Waterloo for providing the experimental data.

References

[1] Inkol et al., 2020. *Multibody Syst Dyn*. 50: 435–452.
[2] Nasr et al., 2021. *J Neural Eng.* 18: 0460d3.
[3] Dumas et al., 2007. *J Biomechanics*. 40: 543–53.
[4] Nasr et al., 2021. In *Proceedings of ASB2021*. 84.
[5] Nasr et al., 2021. *Front. Comput. Neurosci*. 15: 759489.

MEASURING THE CONTRALATERAL LIMB IS NOT AN ADEQUATE REHABILITATION GOAL FOR ASSESSING MUSCLE FUNCTION IN AN ACL INJURED PEDIATRIC POPULATION

Blake S. Miller[1], Joana F. Hornestam[2,3], Sasha Carsen[2], Daniel L. Benoit[1,3*]
[1] School of Human Kinetics, University of Ottawa, 125 University, Ottawa, ON K1N 6N5, Canada
[2]Children's Hospital of Eastern Ontario, 401 Smyth Road, Ottawa, ON K1H 8L1, Canada
[3]School of Rehabilitation Sciences, University of Ottawa, 451 Smyth Road, Ottawa, ON K1H 8M5, Canada
email: *dbenoit@uottawa.ca

Introduction

The anterior cruciate ligament (ACL) is the most injured ligament in the knee, and the rate is rising in the pediatric population[1]. Typically, when attempting to quantify any deficit of the injured limb, the contralateral limb serves as the reference point[2] for identifying functional capacity and readiness for return to sport. However, given the period of inactivity prior to ACL reconstructive surgery, both limbs, including the contralateral limb, are often weakened, and may not be the best control to the injured limb[3]. Furthermore, there is little information about fatigue resistance in the ACL injured population, and this may be an important factor when evaluating functional capacity.

The aim of this study was therefore to evaluate the strength and fatigue resistance of youth with and without ACL injury to identify whether the non-injured limb of the ACL injured group is suitable to assess functional capacity. To quantify this, differences in isokinetic knee extension, and the corresponding quadriceps activation, during a sustained fatiguing task, were examined.

Methods

112 paediatric participants (44 males and 68 females, mean age 14.2 years) were divided into two groups: participants with a confirmed ACL tear (ACLi, n = 52), and puberty- and activity-level matched control participants with no prior history of knee injuries (CON, n = 60). Participants completed a series of 44 repetitions of isokinetic knee flexion and extension at 90 deg/ sec using a Biodex dynamometer (Biodex Medical Systems Inc, Shirley, New York). Surface EMG sensors (Delsys Incorporated, Natick, MA) simultaneously recorded the quadriceps and hamstring activations. The change in extension torque and quadriceps activation were calculated using the percent difference between the mean of the first five trials, and the mean of the last five trials.

The healthy limb of the ACLi and the dominant limb of the CON were compared using a paired samples t-test. The mean differences (MD) and 95% confidence interval ($CI_{95\%}$) were also reported.

Results and Discussion

There was a significant difference between the change in extension torque in the ACLi group, and the CON group (MD = -0.106, $CI_{95\%}$ = -0.168, 0.044). There was no significant difference in change in flexion torque between the ACLi group and the CON group (MD = -0.045, $CI_{95\%}$ = 0.114, 0.240). There was a significant difference for quadriceps change (MD = 0.141, $CI_{95\%}$ = 0.0343, 0.237), and a significant difference for hamstrings change (MD = 0.125, $CI_{95\%}$ = 0.0044, 0.245).

Table 1. Independent samples t-test results for various changes

	ACLi	CON	*p*
Extension change	0.333± 0.163	0.227 ± 0.164	.001*
Flexion change	0.315 ± 0.178	0.269 ± 0.186	0.199
Quads change	-0.260 ± 0.281	-0.119 ± 0.227	0.004*
Hams change	-0.098 ± 0.321	0.027 ± 0.316	0.042*

Results are reported as mean and standard deviation. ACLi: ACL injured group. CON: uninjured group. *p*: *p*-values. *$p < 0.05$

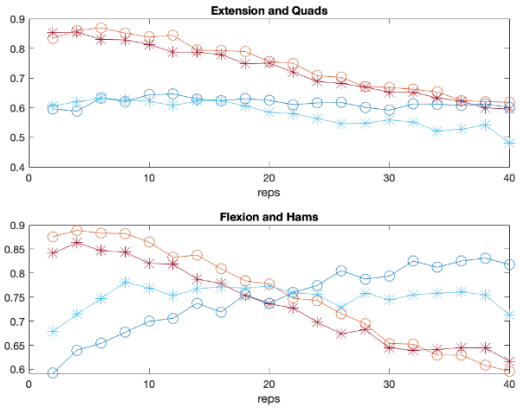

Figure 1: **A)** Average extension (red circles = ACLi, red stars = CON) and quadriceps activation (blue circles = ACLi, blue stars = CON) and B) Average flexion (red circles = ACLi, red stars = CON) and hamstrings activation (blue circles = ACLi, blue stars = CON).

The ACLi contralateral limb had a greater increase in activation despite the decrease in torque when compared to the CON limb. There was no difference in the change in flexion torque however ACLi activation increased.

This leads to two conclusions: (i) ACLi participants' quadriceps and hamstrings are fatiguing faster to output the same level of torque as the CON group with their contralateral leg; (ii) the extension torque of the ACLi group decreased more quickly than the CON group, emphasizing the presence of fatigue. These results are evidence that the contralateral limb of the ACLi cohort does not have the same functional capacity of their non-injured puberty and activity matched controls.

Significance

This study provides clear evidence that the contralateral limb of an ACLi youth cannot be assumed to have the functional capacity of the comparable non-injured population. This is particularly relevant when one considers return to play criteria, since the ACLi participant will be expected to compete with that healthy cohort. The aim in rehabilitation for youth should therefore include a comparison to the healthy puberty- and activity-matched population.

Acknowledgments

We would like to acknowledge Nicholas Romanchuk for his assistance with data analysis.

References

[1] Herzog, M. M., et al. (2018). Sports Health **10**(6): 523-531.
[2] Wellsandt, E., et al. (2017). J Orth Sports Phys Ther **47**(5): 334-338.
[3] Hiemstra, L. A., et al. (2007Clinical Biomechanics **22**(5): 543-55

IMPACT OF THROWING ARM ISOMETRIC STRENGTH ON THRWOING VELOCITY OF COLLEGIATE BASEBALL PITCHERS

Motoki Sakurai[1] and Andrew Karduna[1]
[1]Department of Human Physiology, University of Oregon
Corresponding author's email: motokis@uoregon.edu

Introduction

Overhead throwing is considered one of the most explosive human body motions [1], requiring both high and rapid force producing capacity to enhance throwing performance. Previous studies have reported that higher peak muscle strength of the throwing side shoulder is associated with higher throwing velocity [2,3]. However, to our knowledge, no previous study has examined how neural control of the shoulder muscles, which enables an athlete to produce peak strength within a short time duration, is associated throwing velocity. Rate of force development (RFD) assesses such explosiveness of a muscle, as it derives from the force-time curve and takes the ratio of force development over a given time period at the initiation phase of a motion [4]. Thus, more rapid motor unit firing is required to achieve a greater RFD [4].

The purpose of this study was to examine how both upper extremity strength and RFD are associated with throwing velocity in collegiate athletes. It was hypothesized that both of a greater shoulder RFD and peak shoulder strength would result in increased throwing velocity.

Methods

Seventy-five Division I collegiate baseball pitchers (age: 20.5 ± 1.9 yr, height: 1.88 ± 0.50 m, weight: 90.8 ± 7.1 kg) completed two days of testing. The first day consisted of physical measurements and the second involved pitching performance. Physical strength evaluation consisted of measuring grip strength, shoulder external rotation (ER) / internal rotation (IR) strength, and shoulder scaption strength of their throwing arm. A hand dynamometer (Jamar® Smart Hand Dynamometer, Performance Health, Warrenville, IL, USA) and a portable dynamometer (microFET®2, Hoggan Science, LCC, Salt Lake City, UT, USA) were used for the grip strength and the other strength measurements, respectively. Participants were instructed to squeeze or push the dynamometers with their maximum effort. The mean of two trials for each strength measurement was used for data analysis. For the pitching evaluation, throwing velocity was measured using a radar gun (Stalker Sport 2 radar, Stalker Sport, Richardson, TX, USA) set behind a catcher during a bullpen pitching. Participants were instructed to throw fastballs with their 75% effort for the first 5 pitches and with their maximum effort for the other 5 pitches. The mean of the 5 pitches with the maximum effort was used for data analysis. A multiple linear regression analysis was performed to identify the relationship of the dominant arm muscle strength variables to throwing velocity (SPSS 27, IBM).

Results and Discussion

A multiple linear regression model revealed that all arm strength variables, including both peak strength and RFD, were not significant predictors for throwing velocity ($r^2 = 0.069$, $p > .05$).

Given the results, motor unit firing rate of dominant shoulder muscles may not play an important role in increasing throwing velocity of collegiate baseball pitchers, as any shoulder RFD did not significantly impact throwing velocity in the linear regression model created in the current study.

Although peak strength variables were previously reported to correlate with throwing velocity[2,3], these variables did not show significant association in our linear regression model. This could be attributable to a difference in the methods for assessing shoulder rotational strength. Previous studies examined isokinetic strength to evaluate shoulder IR and ER [2,3], while the current study evaluated shoulder isometric strength.

A limitation of this study was not all participants were fully ready to throw in bullpen because they had just started their fall training after coming back from summer ball league or vacation.

Table 1: Linear multiple regression analysis for the strength-elbow torque relationship ($r^2 = .262$, $p > .05$).

Variables	Coefficient Beta	*P*
Constant	1.665	.00
Peak grip Strength (N)	.003	.33
Peak shoulder ER (N)	.009	.81
Shoulder ER RFD (N/s)	.001	.44
Peak shoulder IR (N)	-.244	.13
Shoulder IR RFD (N/s)	.154	.36
Peak shoulder scaption (N)	.040	.79
Shoulder scaption RFD (N/s)	-.085	.57

Significance

To the best of the author's knowledge, this is the first study that incorporated RFD besides peak strength into physical strength measurement and examined their relationship with throwing velocity of baseball pitchers. Future research is expected to further investigate this relationship.

In conclusion, although the current study failed to observe any significant association in motor unit function of throwing arm with baseball pitching performance, more research is warranted to better understand overhead throwing performance from the neurological perspective.

Acknowledgments

This project was supported by PAC12 Student-Athlete Health and Well Being Grant.

References

[1] Sgroi & Zajac. 2018. *Curr Rev Musculoskelet Med*. 2018;11(1):12-18.
[2] Bayios et al. *J Sports Med Phys Fitness*. 2001;41(2):229-235.
[3] Clements, Ginn, & Henley. 2001. *Physical Therapy in Sport*. 2(3):123-131.
[4] Maffiuletti et al. 2016. *Eur J Appl Physiol*. 116:1091-1116.

PREDICTING THE IMPORTANCE OF THE PSOAS MUSCLE ON WALKING FUNCTION FOLLOWING PELVIC SARCOMA SURGERY

Marleny M. Vega[1*], Geng Li[1], Mohammad S. Shourijeh[1], Di Ao[1], Robert C. Weinschenk[2], Carolynn Patten[3], Josep M. Font-Llagunes[4], Valerae O. Lewis[5], Benjamin J. Fregly[1]
[1]Department of Mechanical Engineering, Rice University, Houston, TX, United States
[2]Department of Orthopaedic Surgery, University of Texas Southwestern Medical Center, Dallas, TX, United States
[3]Department of Physical Medicine and Rehabilitation, University of California, Davis, CA, United States
[4]Department of Mechanical Engineering, Polytechnic University of Catalonia, Barcelona, Spain
[5]Department of Orthopaedic Oncology, University of Texas MD Anderson Cancer Center, Houston, TX, United States
email: *ma86@rice.edu

Introduction

An emerging option for internal hemipelvectomy surgery is custom prosthesis reconstruction to replace the resected pelvic anatomy and hip joint. In theory, a custom prosthesis should produce the best post-surgery walking function. However, the current custom prosthesis design process does not account for surgical or rehabilitation decisions or for post-surgery loading patterns. Patient-specific neuromusculoskeletal models provide one option for predicting the complex interaction between custom pelvic prosthesis design and post-surgery walking function. Although several studies have predicted different gait impairments using personalized models, few research groups have used such models to optimize surgical or rehabilitation decisions. As a first step toward developing this capability for individuals receiving an internal hemipelvectomy with custom prosthesis reconstruction, this study predicted the impact of operated side psoas muscle strength on post-surgery walking function.

Methods

Walking data collected previously from a healthy male subject were used for this study. A neuromusculoskeletal model of the subject was created by personalizing four model elements: joint models, muscle-tendon models, foot-ground contact models, and a neural control model using the concept of muscle synergies; see [1] for details.

The subject-specific model was used in a direct collocation optimal control problem to predict the impact of operated side psoas muscle strength on post-surgery walking function. The post-surgery walking prediction problem was formulated to emulate the most common surgical scenario encountered at MD Anderson Cancer Center in Houston assuming a custom prosthesis design that recapitulated the original pelvis bony anatomy and hip center location on the left leg. Simulated post-surgery psoas strengths included 0% (removed), 50% (weakened), 100% (maintained), and 150% (strengthened) of the pre-surgery value.

Results

Each of the four post-surgery walking predictions achieved a complete gait cycle possessing shorter, quicker, and wider steps than pre-surgery measurements along with a large lateral trunk lean to the operated side (Figure 1). These changes were of comparable magnitude regardless of simulated post-surgery psoas status.

Discussion

Overall, our post-surgery walking predictions were relatively insensitive to post-surgery psoas strength. However, all four situations produced physically realistic walking motions that were generally consistent with clinical observations. Although these results suggest that retention or strengthening of the psoas muscle on the operated side may not be crucial for maximizing post-surgery walking function, future studies are needed to evaluate our predictions using experimental walking data collected post-surgery.

Significance

Gaining confidence in our walking predictions through experimental validation could ultimately allow this computational approach to influence surgical, rehabilitation, and implant design decisions to meet the unique clinical needs of pelvic sarcoma patients.

Acknowledgments

This work was funded by the Cancer Prevention and Research Institute of Texas under grant RR170026 and by an NSF Graduate Research Fellowship.

References

[1] Meyer, A et al. (2016). Frontiers in Bioeng and Biotech, 4:77.

Figure 1: Animation strip comparing the subject's experimental (translucent skeleton) and predicted (opaque skeleton) walking motion when post-surgery psoas strength was 100% of the pre-surgery value.

COMPARING SIMULATION APPROACHES USED IN FINTIE ELEMENT MODELLING OF A MEDIAL OPENING WEDGE HIGH TIBIAL OSTEOTOMY

Victor A. Carranza[1*], Ryan Willing[1,2], Alan M. Getgood[3], Timothy A. Burkhart[4*]
[1]Scool of Biomedical Engineering, Western University, Canada, [2]Department of Mechanical and Material Engineering, Western University, Canada, [3]Fowler Kennedy Sports Medicine Clinic, Western University, Canada, [4]Faculty of Kinesiology and Physical Education, University of Toronto, Canada
email: *timothy.burkhart@utoronto.ca

Introduction

Finite element (FE) modelling has been widely used in research related to medial opening wedge high tibial osteotomy (MOWHTO) of the knee to investigate the stress and strain patterns in the proximal tibia, plate, and screws [1]. There are, however, elementary aspects of modelling MOWHTO in a FE modelling study that must be addressed. In previous studies, the osteotomy cut has been performed in one of two ways (Figure 1): i) the clinically relevant method (CRM) - open the tibial wedge through simulation of the intra-operative procedure [2]; or ii) the simplified method (SM) - cut out the tibial wedge to the desired correction angle without performing the opening [3]. It is unclear however, whether the simplified method accurately describes the intra- and post-surgical biomechanical environment.

The purpose of this study, therefore, is to determine whether the simplified method is an acceptable assumption for a MOWHTO FE modelling study when analysing the stresses and strains in the proximal tibia, plate, and screws.

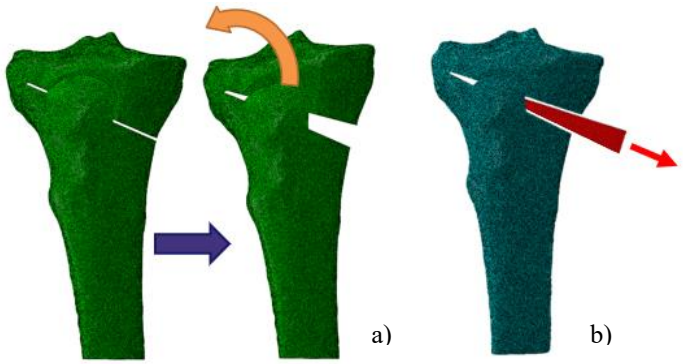

Figure 1: a) CRM where the osteotomy was created through the interoperative opening of the proximal tibia and b) SM where the wedge was removed from the tibia.

Methods

Seven tibia models were reconstructed from CT scans of seven cadaveric specimen. The solid 3D geometry of the tibia was reconstructed in Mimics. Two sets of models were created from the same set of specimens to create the CRM (n=7) and SM (n=7) dataset. The osteotomy in the CRM was simulated by virtually creating an osteotomy cut whose orientation and thickness correspond to the angle and kerf of the osteotomy saw blade. The model was then imported into Abaqus and meshed using an element size of 1.2mm. An image-based CT density mapping approach was used to apply element-specific material properties to the bone. The wedge opening was simulated by pushing apart the edges above and below the saw cut, at the medial face, by 10mm. For the SM, the osteotomy was simulated by simply removing a wedge from the proximal tibia that matches the void normally created by a 10mm opening height, without changing the tibial geometry. Once the osteotomies were created, a simplified Tomofix fixation plate and screw system were modelled and fixed to the tibia to maintain the position of the wedge. The models were then loaded to one bodyweight, distributed evenly across the tibial plateau (50% each on the medial and lateral compartments) with the distal tibia fixed.

Results and Discussion

No statistically significant difference in the micromotion of the osteotomy or the mean plate strains were found. A statistically significant difference in the mean plate stresses was found, with the CRM experiencing 12% greater stresses through the plate construct. A statistically significant difference in mean screw strains and stresses were found between the CRM and SM with the CRM experiencing up to 83% and 47% more strain and stresses, respectively. No differences in strain or stress were found in the proximal tibia near the apex of the osteotomy.

The differences reported here highlight the importance of selecting modelling parameters that best represent the clinical scenario. One explanation for these differences is that the long axis of the tibia was used as a reference for the directionality of the loading condition. With the clinically relevant model, the proximal wedge is moved from its original position, virtually shifting the loading axis to point towards the medial tibia, and therefore towards the plate and screws. This may have caused an increase in the stresses and strains in the plate and screws in the CRM. Similarly, the SM does not account for the geometric changes in the tibia due to the MOWHTO which may underestimate the stresses and strains in the plate and screw construct. Secondly, the positioning of the plate in the SM is more proximal on the tibia due to the lack of bone stock (i.e., the wedge was cut out of the tibia). This creates an unrealistic plate and screw position on the SM. To further improve the models, the element pre-stress calculated because of the opening simulation will be modelled in the CRM which includes plasticity.

Significance

Selecting the appropriate modelling method that best represents the clinical scenario is a crucial step in creating a representative FE model. This study provides an evidence-based approach in the methods to create the osteotomy in a MOWHTO FE modelling study. To account for the mechanical change in a MOWHTO, it is recommended to perform the opening (CRM) of a MOWHTO FE modelling study when analysing the stresses and strains in the plate or screws.

Acknowledgments

This study was funded by the natural sciences and engineering research Council (NSERC), the Western Bone and Joint Institute

References

[1] Burkhart et al, 2013. *J Biomech*. 46(9): 101016. [2] Yang et al, 2021. *PloS ONE*. 16(2): 101371. [3] Golovakha et al, 2014. *BMC Musculoskelet Disord.* 15(230): 101186.

PRE- AND POST-THR TRACKING OF THE VON-MISES STRESSES INDUCED AT SPECIFIC PATHS OF THE FEMORAL SHAFT DURING WALIKING AND STAIR CLIMBING

Wissal Mesfar[1*] and Mohamed Z. Bendjaballah[1]
[1]Biomedical Technology Department, College of Applied Medical Sciences, King Saud University, Riyadh, Saudi Arabia
email: wmesfar@ksu.edu.sa

Introduction

The prediction of stress shielding, defined as a bone loss due to a lack of load in the bone, constitutes a debatable subject in the literature. Many authors shed light on the validity of the prediction of bone remodelling whether stress or strain energy density (SED) was used constituting both strong candidates for the bone stimuli. Others used the stress shielding ratio (SSR) to localize the regions prone to bone resorption. The success of any used method requires the precise prediction of the strain and stress quantities at the specific bony regions. Moreover, the success in the prevention of the stress shielding requires the minimization of the stress decay in the bone. The design of the implant, its material and activities post-THR are the key factors to minimize bone loss and stress shielding. In this study, we aim to use our finite element models of an intact and implanted proximal femoral bone to accurately investigate the von Mises stress variation running along specific paths identically demarcated in both pre- and post-THR models under both walking and stair climbing loading cases. We hypothesise that the stair climbing activity after a post-THR may reduce the risk to develop the stress shielding in the femoral bone.

Methods

An intact and prosthetic 3D FE model of a proximal femur was developed from series of CT-scan images of a left healthy female donor. The bone tissues and prosthesis constituting the FE models were all meshed using hexahedral solid elements. Orthotropic and isotropic material properties were assigned to the cortical and cancellous bone tissues, respectively while 'Ti–6Al–4V' Titanium alloy was chosen for the prosthesis material [1]. A bonded contact was adopted between the prosthesis and bone tissues while a fixed boundary condition was set to the bottom surface of the cortical bone segment. Loading conditions characteristic of walking and stair climbing activities reported by Heller et al. [2] were implemented in the forthcoming FE analyses considering our subject's body weight of 700N. Static nonlinear analyses were performed using Abaqus 6.14 FE software. Nodal von Mises stress distributions were computed along twelve identical paths running through bone shaft of the intact and implanted models. Four cardinal locations were considered, namely the lateral, medial, ventral and dorsal. On each of these locations, three distinct paths at the inner, middle and outer locations were further demarcated over the cortex thickness. Direct comparison of the von Mises stresses computed along each path was performed for the pre- and post-THR condition for both walking and stair climbing activities.

Results and Discussion

The von Mises stresses plotted along the selected tracks were found to be higher on paths belonging to the outer cortex regardless of the model cases. The highest peak stresses of around 50MPa and 60~80MPa were computed on lateral and dorsal path for the walking on dorsal path in stair climbing, respectively, close to the Vastus Lateralis attachment site and distally near the model's bottom face. The results clearly show that the stair climbing increases the stress in the bone in comparison to the walking at the distal site of the femoral shaft but this gradient decrease substantially in the proximal sites of the femoral bone. in all paths except dorsal. Figures 1a and 1b clearly show the previous aspect of this finding. The comparison between the pre- and post-THR stress variations indicates that the medial path at the proximal sites show the highest decay in the stress making this site more prone to develop stress shielding. Moreover, the stair climbing activity doesn't seem to improve the situation at this medial site, since the stress remained almost unchanged.

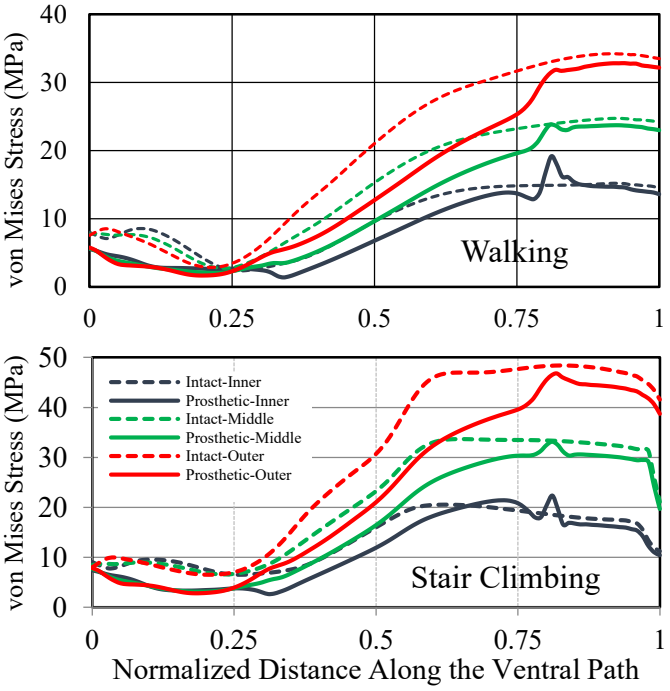

Figure 1: von Mises stresses distribution in the cortical bone for the intact and implanted models under walking and stair climbing loading along three femoral ventral paths.

Significance

In this study the gradient of stress in the femoral bone can be quantified with high accuracy between the pre- and post-THR models under walking and stair climbing loading cases. The stress gradient is a determinant parameter in the determination of the sites prone to bone loss and in the stimulation of the bone remodelling. Its accurate determination is crucial for the success of the mathematical models predicating the evolution of the bone remodelling.

References

1.Piao C, et al. J Orthop Surg Res 9, 7, 2014.
2.Li Y, et al. J Med Biomech 11, 140–143, 1996.

PRELIMINARY VALIDATION OF A PATIENT-SPECIFIC COMPUTATIONAL NEUROMUSCULOSKELETAL MODELLING PIPELINE FOR PATIENTS WITH MEDIAL TIBIOFEMORAL COMPARTMENT KNEE OSTEOARTHRITIS

Dominique S. Cava*, Trevor B. Birmingham, Kristyn M. Leitch, and Ryan Willing
Western University
Corresponding author email:*dcava2@uwo.ca

Introduction

The pathogenesis of knee osteoarthritis (OA) is complex and includes aberrant mechanical loads across the tibiofemoral joint during ambulation. Although joint loads cannot be directly measured in the intact knee, patient-specific EMG-assisted computational neuromusculoskeletal (NMSK) models offer a means to estimate these loads. As it is difficult to validate results in vivo in patients with knee OA, the accuracy of the modelled results must be evaluated before they are interpreted.

Therefore, the purpose of this study was to validate preliminary results from a patient-specific computational neuromusculoskeletal modelling pipeline in patients with moderate knee osteoarthritis.

Methods

Three patients (age = 53 ± 4 years; 2 males and 1 female) were recruited from the Fowler Kennedy Sport Medicine Clinic. All had symptomatic and radiographic (KL grade 2 or 3) knee OA, primarily affecting the medial compartment of the tibiofemoral joint, and varus knee alignment (5.1°±1.9°) based on hip-to-ankle standing radiographs. Kinematic and kinetic data were collected as patients walked barefoot at their self-selected pace for an average of five trials. Electromyography (EMG) data were also collected from the rectus femoris, vastus lateralis and medialis, lateral and medial hamstring, lateral and medial gastrocnemius, and tibialis anterior muscles.

The frontal plane knee alignment of a generic OpenSim model [5] was first adjusted to match the subject-specific knee alignments as it is not a degree of freedom that is available during the scaling of this model. The model was then scaled to the patients' anthropometrics. Gait kinematic and kinetic data were then provided as inputs to inverse dynamics analyses using the subject-specific models. With the results from the inverse dynamics analysis and the corresponding experimentally collected muscle activations, patient-specific EMG-assisted computational NMSK models were then executed in the Calibrated Electromyography Informed NMS Modelling Toolbox (CEINMS) using the EMG-assisted NMSK control mode. The EMG-assisted NMSK control mode adjusts EMG linear envelopes that may be subject to measurement errors and uncertainties, and estimates excitation patterns for musculotendon units from which EMGs cannot be experimentally recorded; all while simultaneously ensuring dynamical consistency in the predicted joint moments. Computed muscle activations and net muscle torques (internal knee flexion torques) were then compared to corresponding experimental muscle activations and OpenSim computed external torques.

Results and Discussion

The root mean square error (RMSE) between the computed and experimental muscle activations for all muscles (%MVIC) was 0.14. Previous literature examining healthy participants and patients with hip OA have cited a RMSE of approximately 0.05 for muscle activation errors. Although our modelled errors were up to 64% higher than values presented in the literature, muscle activations can have a wide range between 0-100 %MVIC. Therefore, we believe these results still provide good agreement between experimental and computed muscle activations with a low RMSE.

The RMSE between internal and OpenSim computed external knee flexion torques (Nm) was 0.18. Previous literature has reported average knee flexion torque errors of less than 0.17. Although our modelled result errors were 6% higher than previous literature, once again, the RMSE was low considering the average knee flexion torque range within this current study was 0-50 Nm. Therefore, these results suggested good agreement between external and internal torques.

Patient-specific computational NMSK models offer a means to calculate the magnitude of loading across the tibiofemoral joint. Before performing these calculations, however, assessing the validity of preliminary modelled results upstream can provide information regarding the accuracy of the data that will be used to calculate joint distribution. Results of this study demonstrate good agreement when compared to previous literature including healthy participants and patients with hip OA that follow a similar computational NMSK modelling pipeline. Therefore, preliminary results suggest this current patient-specific NMSK modeling pipeline can accurately predict muscle activations and knee joint torques in patients with medial tibiofemoral compartment knee OA.

Significance

Knee OA is associated with aberrant ambulatory mechanics, including the magnitude, distribution, timing of loads, and neuromuscular control. Patient-specific computational NMSK modelling such as the present pipeline is important to better understand knee OA progression, and develop and evaluate potential interventions.

Acknowledgments

This research was supported by a Catalyst Grant from Western University's Bone and Joint Institute.

References

[1] Hoang et al., 2019. *J Biomech*. 83: 134-142.
[2] Mootanah et al., 2014. *Comput Methods Biomech Miomed Engin*. 17: 1502-1517.
[3] Pizzolato et al., 2016. *J Biomech*. 48: 3929-3936.
[4] Sartori et al., 2014. *J Biomech*. 47: 3613-3621.
[5] Saxby et al., 2016. *Gait Posture*. 49: 78-85.
[6] Sritharan et al., 2017. *J Orthop Res*. 35: 321-330.

Quantification of Load Distribution on the Hand and Fingers

Paul M. Tilley, Ryan Chhiba, Peter J. Keir*
Department of Kinesiology, McMaster University, Hamilton, ON, Canada, L8S 4K1
*Corresponding Author Email: pjkeir@mcmaster.ca

Introduction

The hand is our primary tool for interacting with the external environment and is exposed to combinations of mechanical loads. Biomechanical models are often employed to calculate internal joint moments and muscle forces under external loads. The generalizability of the hand models does not typically account for individual differences in load distribution and contact areas during hand-object interactions (1). The purpose of this study was to quantify the load distribution within the hand during common grasps.

Methods

Due to COVID-19 restrictions, analysis is currently limited to two participants. Each participant completed five trials for each grasp. Hand pressures during four tasks were quantified: (i) medium wrap, (ii) lateral pinch, (iii) three finger chuck, and (iv) table lean. The Tekscan™ Grip System (Tekscan, Inc., South Boston, MA) is a pressure mapping system equipped with 17 regional sensors. Each grasp was held for five seconds and sampled at 60 Hz. The pressures measured by each sensor were averaged for each trial. This work will be expanded to a larger group of participants and tasks. Dynamic tasks will be analyzed using statistical parametric mapping.

Results and Discussion

The mean load distributions of the four hand tasks are presented as a percent of the total hand load (Figure 1). Although load distribution differs across all four actions, some commonalities were identified. Generally, loading was greater on the distal phalanges than on the proximal phalanges. Load distribution was also greatest at the distal thumb in the medium wrap, lateral pinch, and 3 finger chuck grasps. During the medium wrap grasp, loading was greater on the middle finger than the index, ring, and little fingers. During the lateral pinch, loading is greater at the thumb than in the index finger. However, index finger loading may not be representative for the lateral pinch as there are no sensors on the lateral surface of the fingers. During the 3-finger chuck grasp, loading was greater in the index finger than the middle finger. When the hand was used for support in the table lean, loading was concentrated over the carpals, with minimal loading over the metacarpals and fingers.

These preliminary results indicate that load distribution on the hand during grasping tasks differs depending on the posture of the hand. This work is planned to expand with a larger sample size that encompasses a variety of hand anthropometrics, additional common grasps, and kinematics of the forearm, hand and fingers. The findings will provide a more robust understanding of how loads are distributed during hand-object interactions.

Significance

This work will aid in the quantification of loading during hand object interactions. The role of load placement and distribution at the hand will facilitate in improving our understanding of internal loading and injury mechanisms. The knowledge can be applied to current biomechanical models of the hand to improve the representation of internal loading during activities of daily living and occupational tasks.

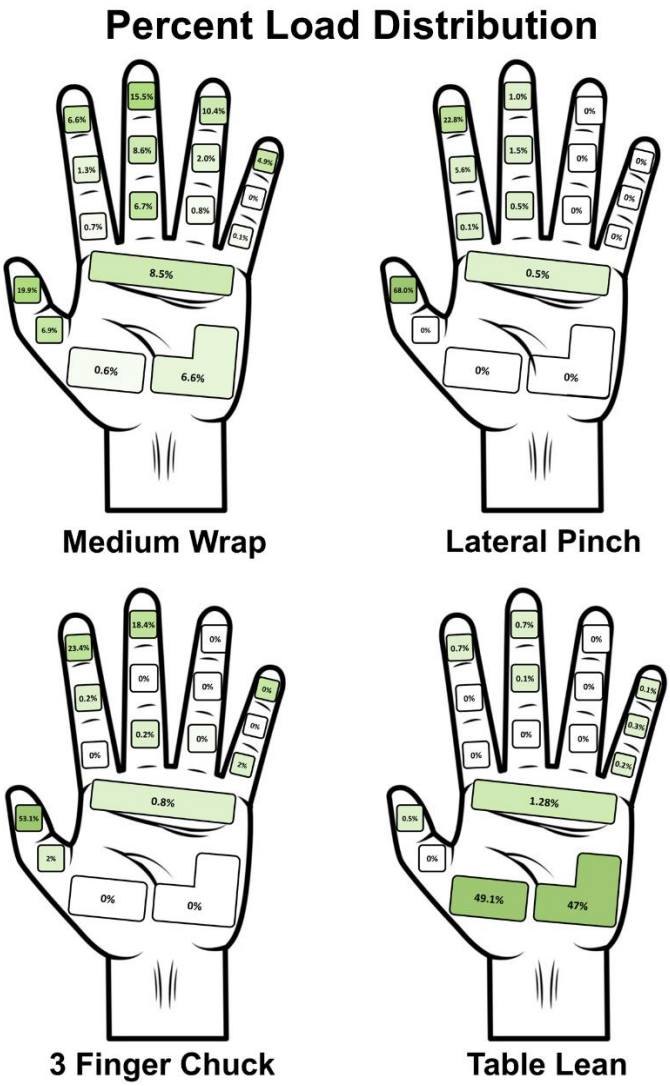

Figure 1: Percent load distribution on each sensor for medium wrap (top left), lateral pinch (top right), 3 finger chuck (bottom left), and table lean (bottom right). Darker shading indicates a greater proportion of the load.

Acknowledgements

NSERC Discovery Grant (RGPIN-2016-06460)

References

1) Komi, E. R., Roberts, J. R., & Rothberg, S. J. (2008). Measurement and analysis of grip force during a golf shot. Proceedings of the Institution of Mechanical Engineers, Part P: Journal of Sports Engineering and Technology, 222(1), 23–35. https://doi.org/10.1243/17543371JSET9

DEVELOPMENT OF A CONGRUENCE-BASED MUSCULOSKELETAL MODEL OF THE KNEE IN ANTERIOR CRUCIATE LIGAMENT INJURED ADOLESCENTS

Claire E. Warren[1], Michele Conconi[2], Nicola Sancisi[2], Sasha Carsen[3] and Daniel L. Benoit[4]
[1]School of Human Kinetics, University of Ottawa, Canada
[2]Department of Industrial Engineering – DIN, University of Bologna, Italy
[3]Division of Orthopaedic Surgery, CHEO (the Children's Hospital of Eastern Ontario), Ottawa, Canada
[4]School of Rehabilitation Sciences, University of Ottawa, 451 Smyth Rd, Ottawa, Canada
email: *claire.warren@uottawa.ca

Introduction

Anterior cruciate ligament (ACL) injury rates are rising in adolescent populations [1]. To understand how an individual's joint morphology dictates their motion patterns, researchers have developed patient-specific musculoskeletal models using medical images of the tibiofemoral joint (TFJ) to study ACL injuries [2]. In particular, congruence-based modelling optimizes the configuration of the tibiofemoral joint to reduce pressure during movement [3], mimicking the mechanotransduction properties of articular cartilage [4]. However, these models have predominantly been constructed using adult knees, and it is unclear if patient-specific models can be built for populations undergoing pubertal development. Therefore, the purpose of this research is to build a patient-specific knee model for modelling passive knee joint motion during adolescence.

Methods

Magnetic resonance images (MRI) of 12 ACL-injured (ACL-I) adolescents (6 male, 6 female, Tanner Stage: 3.91 ± 1.2) were used to segment long bones of the tibiofemoral joint with cartilage and menisci. Natural knee motion was determined using an algorithm developed by Conconi et al. (2021) as the envelope of tibiofemoral configurations that maximize joint congruency [5]. Knee flexion was controlled through two degree increments from 6 to 108°. The remaining degrees of freedom (DOF) were optimized for maximized knee joint congruency, inherently minimizing knee joint pressure [5]. Anatomical reference system (ARS) was defined in accordance with Gray et al (2019) , evaluating joint translations through the relative position of ARS origin and orientation through z-y-x cardanic sequence of rotation [6]. Average range of motion (ROM) was calculated as difference between positions at each increased flexion increment with initial position at 6 degrees. Ligament strain (%) was calculated using the Euclidian distance of the most isometric fibre as the resting length for all ligaments. All resultant joint kinematics are expressed from the femur with respect to the tibia.

Results and Discussion

Preliminary data shows successful generation of optimized passive range of motion (ROM) for ab/adduction (AA), internal/external (IE) rotation angles, in addition to anterior/posterior (AP), superior/inferior (SI) and medial/lateral (ML) translations. Average AA and IE ROM were 1.05±0.38° and 6.22±1.8° respectfully. Optimized average AP, SI and ML ROM were 2.16±0.54mm 1.84±0.54mm and 1.840.48mm. Average ligament % elongation for the ACL, PCL, MCL and LCL were 2.47± 1.1%, 6.55± 3.8%, -2.20± 0.9% and 10.6 ± 0.6%.

Larger ROM of IE rotation of the femur could be explained by increases in knee laxity, due to hormone fluctuations caused by the onset of puberty [7].

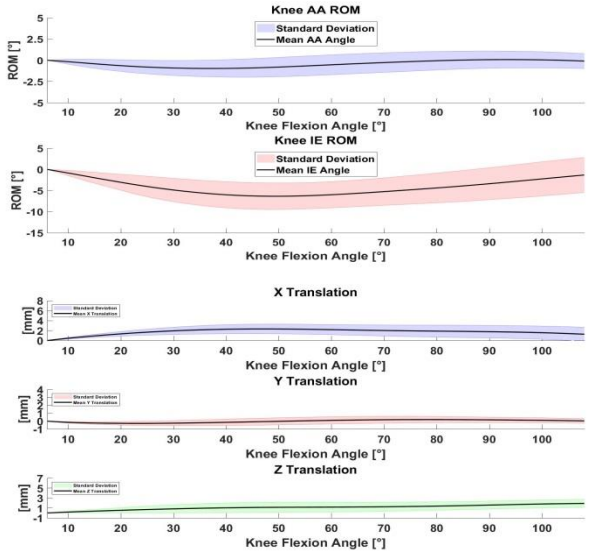

Figure 1: Resultant optimized kinematics for ab/adduction, internal/external rotation, and translations in remaining DOF.

Significance

Inter-subject variability in passive kinematic motion derived from patient-specific morphology highlights the need for personalized musculoskeletal models in growing populations. Congruence-based modelling produces a unique baseline motion for each subject dictated by TFJ articulations, despite variations in pubertal development. Resulting motion can be used to study pathological deviations in kinematics while considering the effects of TFJ articulation on movement patterns. This leads to more comprehensive research on ACL injury and re-injury mechanisms, particularly throughout adolescence.

Acknowledgments

The authors would like to thank the Natural Sciences and Engineering Research Council (NSERC) for the financial support during the completion of this research

References

[1] Herzog et al., 2018. *Sports Health.* 10(6):523-531.
[2] Smale et al., 2019. *J. Biomech.* 83:9-15.
[3] M. Conconi. 2014. *Proc. Inst. Mech. Eng. Part H J Eng. Med.,*228(9), 935-941.
[4] Caravaggi et al., *Front. Bioeng. Biotechnol.* 9 :634327.
[5] Conconi et al., 2021. *IEEE Trans Biomed Eng,* 68(3). 1084-92
[6] Gray et al. 2019. *J. Orthop Res.337:615-630*
[7] Price et al., 2017. *Curr. Opin. Pediatr.* 29(1):55-64

COSIMULATION AND VALIDATION OF INDEX FINGER EXTENSOR HOOD MODELS

*Christopher T. Jadelis[1], Derek Kamper[2], Katherine R. Saul[1]
[1]Department of Mechanical and Aerospace Engineering, North Carolina State University, Raleigh, NC, USA
[2]Joint Department of Biomedical Engineering, North Carolina State University and UNC-Chapel Hill, Raleigh, NC, USA
email: *ctjadeli@ncsu.edu

Introduction

Musculoskeletal modelling has been crucial for exploring the mechanics of dexterity [1], with multibody dynamic (MBD) models used to explore mechanical consequences of hand deformities and disability [2,3]. However, anatomical properties such as the low inertia of finger segments and specialized tissue structures present challenges for hand modelling [4]. For example, the extensor hood mechanism runs along the dorsal side of each finger and transmits forces from multiple muscle tendons. It has heterogeneous mechanical properties and multiple insertions and ligamentous adhesion sites [5]. Finite element (FE) analysis is ideal for this structure, but is computationally expensive for examining coordinated hand motion. Thus, MBD models typically use lumped muscle models. To address these limitations, we present a cosimulation approach for integrating an FE model of the extensor mechanism with an existing MBD model of the hand to preserve the benefits of both approaches.

Methods

An existing MBD model of the hand and fingers in OpenSim [2] and an FE model of the index finger extensor hood implemented in FEBio [6] were adapted for use in this study. The FE model incorporates tendon forces from the four muscles that typically insert into the extensor hood: extensor digitorum communis (EDC), extensor indicis (EI), first palmar interosseous (FPI) and lumbrical of the index finger (LUM). Tendinous insertions of the extensor hood onto the phalanges were used to represent the central slip (CS) and terminal slip (TS) with material properties defined by [5]. Validation was conducted for the FE model to replicate previous cadaver studies [7] in which the EDC had a constant force of 11.8N while finger posture was varied. Net changes in length for the central slip and terminal slip were used to calculate net strains for comparison with experimental data.

Integration between the MBD and FE models was accomplished using a custom MATLAB script (**Fig. 1**). The muscle model in the MBD model was used to generate muscle forces that were applied as initial conditions to the FE model. Resulting joint moments from the FE model were then applied to the MBD model in place of muscle actuators to model the net effect of the extensor mechanism in coordinated motion. Validation of the cosimulation was performed to replicate previous cadaver studies measuring isometric fingertip force production [8]. This was replicated by constraining the MBD and FE models into a set posture with a contact surface placed at the fingertip in the MBD model. Fingertip forces were recorded and compared to experimental data (**Fig. 2b**)

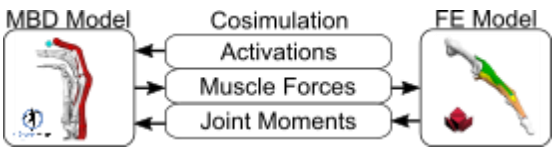

Figure 1. Flow of information in cosimulation

Results and Discussion

Validation simulations of the FE model successfully converged for all postures within the range of experimental results, with a maximum deviation of 0.69%, and 0.91% strain from the experimental results for the CS and TS respectively (**Fig. 2a**). Cosimulation of the index finger extensor hood with MBD and FE models additionally reflected experimental results, with fingertip force magnitudes falling within 0.3N of the experimental results for the EDC, EI, and LUM muscles, and 0.62N for the FPI muscle. Force vectors in the sagittal plane were directed proximally and dorsally for the EDC and EI muscles, and distally and dorsally for the FPI and LUM muscles, similar to experimental results, with a maximum deviation of 29.9° (**Fig. 2b**).

This work demonstrates a generalizable model for simulation of the extensor hood where deformation mechanics and functional changes to extensor mechanism can be explored within the context of coordinated motion of the hand by combining FE and MBD models. Current simulations examine isometric tasks; dynamic tasks and coordinated motions will be explored in future simulations.

Acknowledgements

NSF IIS- 2106747

Significance

These models and cosimulation method enable a new method for examining functional changes due to the contributions of soft tissues within coordinated movement tasks. This work can be applied to examining the impact of disease and injury on dexterity, and predict what functional improvements may result from intervention.

References

[1] M. T. Duruöz, *Hand Function*, 2014, pp. 41–51.
[2] A. J. Barry et al. *J. Biomech*. **77**, pp. 206–210, Aug. 2018.
[3] B. I. Binder-Markey et al. *J. Hand Surg*. **44**, Sep. 2019.
[4] B. I. Binder-Markey et al. *J. Biomech*., **61**, Aug. 2017.
[5] K. Qian et al. *J. Biomech*. **47**, Sep. 2014.
[6] B. Ellis et al. American Society of Biomechanics, 2011.
[7] S. W. Lee, et al. *J. Biomech. Eng*. **130**, Oct. 2008.
[8] D. Qiu. Illinois Institute of Technology, 2014.

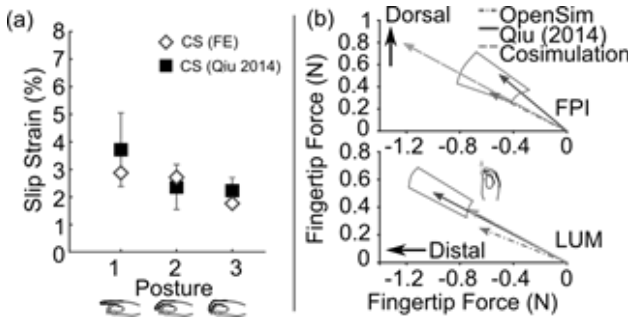

Figure 2. (a) FE model strains, (b) cosimulation forces

LOAD SHARING ASSESSMENT IN A THORACIC FUNCTIONAL UNIT DURING SURGICAL RESECTION

Michael Polanco[1], Stacie Ringleb[1], Michel Audette[1], James Bennett[2], Carl St. Remy[2] and Sebastian Bawab[1]
[1]Old Dominion University, Norfolk, VA USA, [2]Children's Hospital of the King's Daughters, Norfolk, VA USA
email: sbawab@odu.edu

Introduction

Resection procedures of the spine traditionally require removal of osteoligamentous anatomy to achieve sufficient correction for various pathological deformities such as kyphosis and scoliosis. Previous studies have assessed the change in load distribution upon ligament and facet removal in the lumbar spine [1] and within the cervical spine [2]. However, the effects of load distribution within the thoracic spine are not well understood. The presence of the ribcage adds stability and reinforcement to the thoracic column not seen in the other spinal regions and could affect how the spine behaves during surgical resection. Understanding the load distribution within the spinal column may help a surgeon better understand the clinical effects of spinal deformity treatments on a patient-specific basis. The following study examines the load distribution within a thoracic spine functional unit during posterior release.

Methods

A finite element (FE) model of an asymptomatic T7-T8 functional unit was created using geometry from an anatomist-drawn computer-aided drawing (CAD) model of the adult spine (CG Hero Ltd., Manchester, UK) and prepared using Hypermesh (Altair Engineering, Troy, MI, USA). Material properties for the vertebrae and intervertebral disc (IVD) were obtained from the literature [3]. Intervertebral ligament [4,5] and costovertebral (CV) joint ligament properties [6] in the FE model were assigned using tension-only elements. Quasi-static analyses were run using LS-DYNA (Livermore Software Technology, Livermore, CA), where a pure external moment of ±5 N-m was applied over the superior (T7) endplate in flexion and extension. The FE model was first analysed with all spinal components intact. Next, components were serially removed following the sequence consistent with a Ponte osteotomy [7]. For each case, ligament, disc, and contact forces from the facet and CV joint were calculated; each force was then multiplied by the perpendicular moment arm corresponding with the Instantaneous Center of Rotation (ICR) [8], or moment arm origin, to derive the internal moment borne by each component as a percentage of applied external moment. Rotational equilibrium (e.g.: $\sum M_{ICR} = 0$) between the external moment and all internal moments was assumed in all cases.

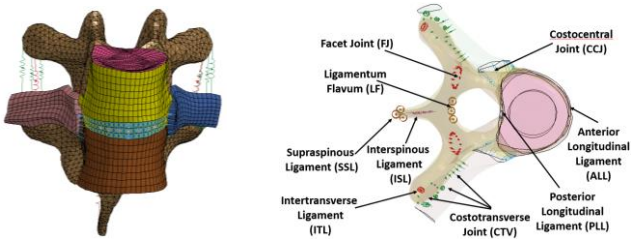

Figure 1: T7-T8 FE model with labeled spine components.

Results and Discussion

In flexion, at the maximally applied moment (Table 1), approximately 76% of the overall internal load is borne by the IVD, Ligamentum Flavum (LF), and intertransverse ligament (ITL) in the intact configuration. The greatest increase is seen within the ITL after the LF is removed by approximately 21%. In extension, at the maximally applied moment, approximately 88% of the internal load is borne by the facet joint (FJ) and IVD intact, with the latter seeing 66% of the load. After the facetectomy is conducted, the load borne by the intervertebral disc increases by approximately 18%.

The anterior shift in ICR [8] can explain the differences in load bearing upon removal of a spinal component [1]. In addition, spinal components that traditionally bear a significant portion of load within the spine, such as the LF in flexion [1] and the FJ in extension [2], are shown to take significant load proportions. Load borne by the CV joint was not shown to be as relatively significant likely due to the absence of the ribcage and could have produced stiffer behavior with its presence. The load distribution is restricted by soft tissue material properties utilized in the FE model as well as the removal sequence. Future work will explore load bearing behavior in lateral bending and axial rotation while exploring the removal sequence sensitivity of the spinal components.

Significance

This abstract describes a method by which surgeons can explore paths to treat thoracic-based deformities safely and effectively such as kyphosis and scoliosis. Surgeons performing a Ponte osteotomy typically remove the spinous ligaments, ligamentum flavum, and portions of the facet joints. Understanding how removing portions of the posterior spinal column affect the overall load distribution within the spine may help surgeons make informed decisions while improving long-term outcomes for their patients.

Acknowledgments

This project was funded by the Children's Research Foundation and a SMART Scholarship received by M. Polanco.

References

[1] Sharma, M. et al., 1995. *Spine* **20**(8), 887-900.
[2] Panzer, M. et al., 2009. *Biomechanics* **42**, 480-90.
[3] Naserkhaki, S. et al. 2018. Biomechanics **70**, 33-42.
[4] Chazal, J. et al. 1985. *Biomechanics* **18**(3), 167-76.
[5] Shirazi-Adl, A. et al., 1986. *Spine* **11**(9), 914-27.
[6] Polanco, M. et al., 2021. ASB Conference, Podium.
[7] Ponte, A. et al., 2018. Spine Deformity **6**, 2-11.
[8] Polanco, M. et al., 2021, ASB Conference, Poster.

Table 1: Load distribution percentages of spinal components in Flexion (left column) and Extension (right column).

	ALL		CCJ		CTV		FJ		IVD		ITL		LF		ISL		SSL		PLL	
Intact	0	0.42	0.03	4.2	4.7	7.5	1.9	21.7	43.9	66.1	16.7	0	15.6	0	8.6	0	9.1	0	0	0
ISL & SSL removed	0	0.42	0.65	4.1	4.6	7.5	3.1	21.7	48.6	66.2	22.2	0	20.9	0	0	0	0	0	0	0
Bilateral Facetectomy	0	0.47	0.98	5.7	4.8	10.0	0	0	48.4	83.8	24.1	0	21.8	0	0	0	0	0	0	0
LF removed	0	0.47	1.5	5.7	5.8	10.0	0	0	47.3	83.8	45.5	0	0	0	0	0	0	0	0	0

COMPARISON OF A SPINE MODEL BETWEEN TWO FINITE ELEMENT PROGRAMS

Isaac K. Kumi, Michael Polanco, Jinhyuk Kim, Sebastian Bawab, Stacie Ringleb
Old Dominion University, Norfolk, VA, USA
email: sringleb@odu.edu

Introduction

Computational models are used in biomechanics to help scientists and clinicians understand complex problems, including but not limited to how joints work in situations where direct measurement is difficult or impossible and the effects of different treatment options. Numerous finite element analysis programs have been used to study different aspects of the musculoskeletal system, making it challenging to compare results generated from different programs. Furthermore, the underlying abilities of many of these programs are different; thus, it can be challenging to recreate a model developed in one program in a different program. However, understanding the differences in finite element software can help researchers understand the limitations in comparing results across software platforms.

FEBio (FEBio, Salt Lake City, UT) is an open-source finite element program explicitly designed to solve nonlinear significant deformation problems in biomechanics and biophysics. LS-DYNA (Livermore Software Technology, Livermore, CA) on the other hand is a general-purpose finite element program designed to conduct transient, dynamic finite element simulations applicable to automotive, aerospace, and bioengineering problems. Both software have been used in biomechanical modelling, but it is unclear if a model made in one program can be easily translated to the other. This study aims to translate a spine model created for use in one finite element (FE) software into another FE software.

Methods

An open-source 3D finite element functional unit model [1] was obtained (Fig. 1) and analyzed in FEBio and LS-DYNA. Material properties [1] of the ligaments and bones were the same in both models. However, the annulus fibres were characterised differently as there was no common method to generate them in both programs. In FEBio, the matrix and the annulus fibres were modelled together as a solid mixture; a Mooney Rivlin material for the matrix and a fibre-exp-pow formulation for the annulus fibres [1]. In the absence of the solid mixture composition in LS-DYNA, a custom-written MATLAB (The MathWorks Inc., Natick, MA) script was used to generate the annulus fibres [3].

Ligaments were modelled as tension-only springs with force-displacement characteristics using human ligament data from literature [4]. A rigid torque of 7500 N-mm was applied on the superior endplate of the L4 vertebrae. All degrees of freedom on the inferior endplate of the L5 vertebrae were constrained. After conducting quasi-static analyses, the range of motion values were obtained for flexion, extension, right lateral bending, and left axial rotation. Symmetric conditions were assumed for lateral bending and axial rotation.

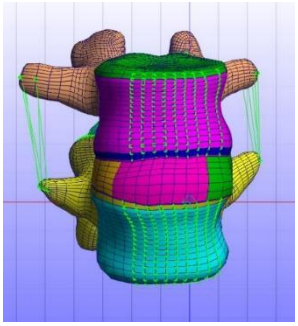

Figure 1: Open -source Finite Element Model of the L4-L5 vertebra

Results and Discussion

Similar ranges of motion values were obtained when results from both software were analyzed (Fig. 2). The results were benchmarked with an in vitro study [5], which were mostly in agreement. There are inherent differences in solvers for both programs that affected the model computation. For example, dynamic-based parameters such as mass density were not required for material characterization in FEBio, but the input was required for time step calculation in LS-DYNA. However, due to the quasi-static nature of both models, no significant kinematic differences were seen between them.

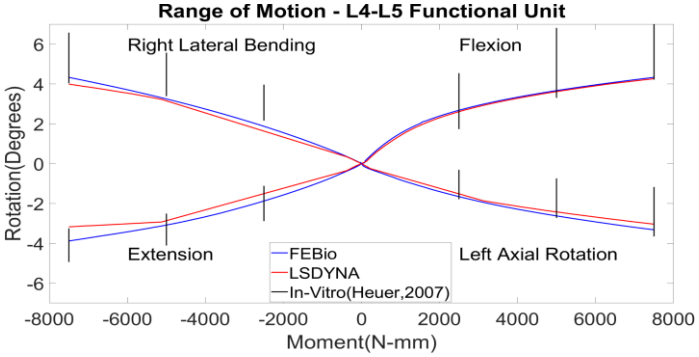

Fig. 2 ROM curves for the L4-L5 functional unit analysed in FEBio and LS-DYNA. The *in vitro* study shows the maximum and minimum range acceptable for 2500 N-mm, 5000 N-mm and 7500 N-mm for all ROM.

Significance

This study has shown that FE models can be utilised in different programs to help verify and validate results. However, to have a smooth translation and a lower error margin, it is necessary to understand how each FE software works and their inherent capabilities.

References

[1] Finley, S. et al. Comp. Method in Biom. 21(6), 444-52, 2018
[2] Jacobs, N.T. et al. Biomechanics 47,2540-46,2014.
[3] Shirazi-Adl, A. et al. Spine 9,120-34, 1986.
[4] Rohlmann, A. et al. Biomechanics 39, 2484-90, 2006.
[5] Heuer, F et al. Biomechanics 40, 271-80, 2007.

Evaluating the Influence of Multiple Pressure Points on the Hand and Fingers

Ryan Chhiba, Nigel T. Majoni, Paul M. Tilley, Peter J. Keir*
Department of Kinesiology, McMaster University, Hamilton, ON, Canada, L8S 4K1
* Email: pjkeir@mcmaster.ca

Introduction

Forces acting on the hand during everyday tasks are complex and necessary to assess the risks of developing hand-related musculoskeletal disorders [1]. Current biomechanical models that are used to calculate internal muscle forces, do not fully consider distribution or multiple areas of contact [2]. Rather than assuming points of contact, a pressure mapping system can provide detailed pressure magnitudes and locations over the palmar surface of the hand. The objective of this study is to determine local Centres of Pressure (CofP) on the fingers and hand during hand actions to use as input for computational modelling to examine how internal tissue (tendon and joint) loads are affected by point of force application.

Methods

Due to the COVID-19 pandemic, analysis is currently limited to 2 participants. A hand pressure mapping system (Tekscan Grip System, TekScan Inc, Boston, MA) was used to collect forces and determine the local CofP in each region of the hand. Each participant completed 5 trials of each task. Data was collected on the right hand during the following 4 tasks: (i) medium wrap around a cylinder (d= 5.1cm), (ii) lateral (key) pinch, (iii) three finger chuck (holding marker), and (iv) table lean. Each action was held for five seconds and sampled at 60 Hz. The mean CofP for each of the sensor regions (Figure 1) were recorded. Statistical parametric mapping will be employed to compare continuous data during dynamic tasks.

Results and Discussion

The mean CofP for each trial is presented over the sensor grid (Figure 1). Grid coordinates were used to visualize the CofP data on each of the 17 regions. The 3-finger chuck and lateral pinch tasks show consistent CofP across trials, while the medium wrap and table lean tasks appear to have greater variation in CofP locations. The lateral pinch task shows greater regional variation in the proximal/distal directions, whereas the table lean, and medium wrap tasks show greater regional variation in the radial/ulnar direction. Further analyses will distinguish the local CofP that occur during hand-object interactions from region-region interaction. CofP results also demonstrate considerable variance in loading patterns between trials of the same action. The extent of the variation will be explored with the recruitment of more participants.

Currently, two male participants have been evaluated due to COVID-19 restrictions for human participants. Further analyses will include sex and hand anthropometrics to reveal whether simple scaling or more detailed methods are needed for modelling. The complete protocol contains a more comprehensive series of static and dynamic hand actions. Further collection will distinguish points of force application for each region. The distribution of loads at multiple sites on the hand and fingers will be used in conjunction with force magnitudes to better inform the needed inputs to describe internal muscle and joint forces in computational models.

Significance

This study provides information on the multiple sites for loads acting on the hand during common human-object interactions. Examining the effect of multiple loading sites as an input to computational models of the hand will lead to better estimates of internal joint and tendon loads, thus improving understanding of injury mechanics in the workplace. The knowledge of this study can be applied to existing biomechanical models of the upper extremity to increase its representation of real-world interactions.

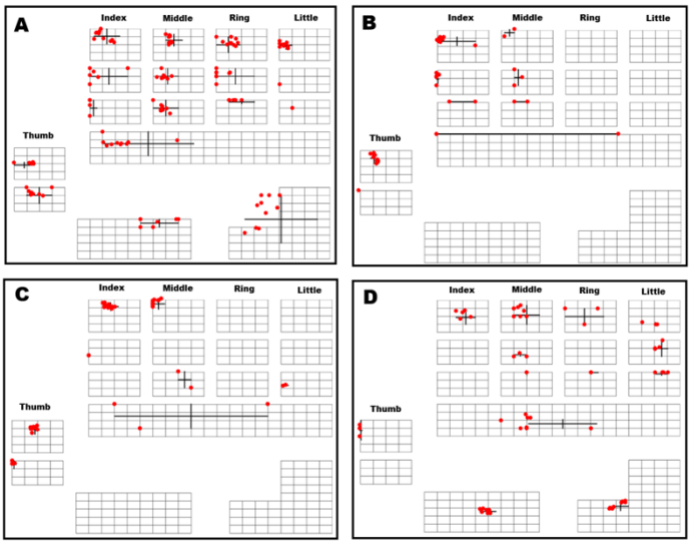

Figure 1: Centre of pressure (CofP) on hand during a medium wrap (A), lateral pinch (B), 3-finger chuck (C), and table lean (D). Each data point represents the mean local CofP for each trial.

Acknowledgements

NSERC Discovery Grant (RGPIN-2016-06460).

References

[1] Sinsel, E.W., Gloekler, D.S., Wimer, B.M., Warren, C.M., Wu, J.Z., & Buczek, F.L. (2016). Automated pressure map segmentation for quantifying phalangeal kinetics during cylindrical gripping. *Medical Engineering & Physics*, *38*(2), 72-79.

[2] Hicks, J. L., Uchida, T. K., Seth, A., Rajagopal, A., & Delp, S. L. (2015). Is my model good enough? Best practices for verification and validation of musculoskeletal models and simulations of movement. *Journal of biomechanical engineering*, *137*(2), 020905. https://doi.org/10.1115/1.4029304